Aspects of thermal and chemical equilibration of hadronic matter [*]

E. L. Bratkovskaya, W. Cassing, C. Greiner,

M. Effenberger, U. Mosel and A. Sibirtsev

Institut für Theoretische Physik, Universität Giessen

35392 Giessen, Germany

Abstract

We study thermal and chemical equilibration in 'infinite' hadron matter as well as in finite size relativistic nucleus-nucleus collisions using a BUU cascade transport model that contains resonance and string degrees-of-freedom. The 'infinite' hadron matter is simulated within a cubic box with periodic boundary conditions. The various equilibration times depend on baryon density and energy density and are much shorter for particles consisting of light quarks then for particles including strangeness. For kaons and antikaons the chemical equilibration time is found to be larger than $\simeq 40$ fm/c for all baryon and energy densities considered. The inclusion of continuum excitations, i.e. hadron 'strings', leads to a limiting temperature of $T_s \simeq 150$ MeV. We, furthermore, study the expansion of a hadronic fireball after equilibration. The slope parameters of the particles after expansion increase with their mass; the pions leave the fireball much faster then nucleons and accelerate subsequently heavier hadrons by rescattering ('pion wind'). If the system before expansion is close to the limiting temperature T_s, the slope parameters for all particles after expansion practically do not depend on (initial) energy and baryon density. Finally, the equilibration in relativistic nucleus-nucleus collision is considered. Since the reaction time here is much shorter than the equilibration time for strangeness, a chemical equilibrium of strange particles in heavy-ion collisions is not supported by our transport calculations. However, the various particle spectra can approximately be described within the blast model.

---

1 Introduction

Nucleus-nucleus collisions at relativistic and ultrarelativistic energies are studied experimentally and theoretically to obtain information about the properties of hadrons at high density and/or temperature as well as about the phase transition to a new state of matter, the quark-gluon plasma (QGP). In the latter deconfined partons are the essential degrees of freedom that resolve the underlying structure of hadrons [1]. Whereas the early 'big-bang' of the universe most likely evolved through steps of kinetic and chemical equilibrium, the laboratory 'tiny bangs' proceed through phase-space configurations that initially are far from an equilibrium phase and then evolve by fast expansion. These 'specific initial conditions' – on the theoretical side – have lead to a rapid development of nonequilibrium quantum field theory and nonequilibribrium kinetic theory [2, 3]. Presently, semiclassical transport models are widely used as approximate solutions to these theories and practically are an essential ingredient in the experimental data analysis. For recent reviews we refer the reader to Refs. [4, 5, 6].

On the other hand, many observables from strongly interacting systems are dominated by many-body phase space such that spectra and abundances look 'thermal'. It is thus tempting to characterize the experimental observables by global thermodynamical quantities like 'temperature', chemical potentials or entropy [7, 8, 9, 10, 11]. We note, that even the use of macroscopic models like hydrodynamics [12, 13] employs as basic assumption the concept of local thermal and chemical equilibrium. The crucial question, however, how and on what timescales a global thermodynamic equilibrium can be achieved, is presently a matter of debate. Thus nonequilibrium approaches have been used in the past to address the problem of timescales associated to global or local equilibration [14, 15, 16, 17, 18, 19, 20, 21]. In view of the increasing 'popularity' of thermodynamic analyses a thorough microscopic reanalysis of this questions appears necessary especially for nucleus-nucleus collisions at ultrarelativistic energies that aim at 'detecting' a phase transition to the QGP.

In this paper we study equilibration phenomena in 'infinite' hadronic matter using a microscopic transport model that contains both hadron resonance and string degrees-of-freedom. With this investigation we want to provide insight into the reaction dynamics by the use of cascade-like models and also point out some of their limitations. The 'infinite' hadronic matter is modelled by initializing the system solely by nucleonic degrees of freedom through a fixed baryon density and energy density, while confining it to a cubic box and imposing periodic boundary conditions during the propagation in time. We, furthermore, then study the expansion of the hadronic fireball after equilibration to investigate the changes in hadron spectra during the rapid explosion as well as related equilibration phenomena in realistic nucleus-nucleus collisions for light and heavy systems.

Our paper is organized as follows: In Section 2 we briefly describe the approach

employed in our investigations, specify the initial conditions for a finite box with periodic boundary conditions, present our numerical results and extract various (hadronic) equilibration times as well as thermodynamical properties for different initial conditions. Section 3 is devoted to the expansion dynamics of the equlibrated fireball and a discussion of the related physical phenomena. In Section 4 we analyse reactions of colliding finite light and heavy systems and compare our result to a blast model. Section 5 concludes our study with a summary.

2 Equilibration and limiting temperature

To investigate the equilibration phenomena addressed above we perform microscopic calculations using the Boltzmann-Uehling-Uhlenbeck (BUU) model of Refs. [23, 24]. This model is based on the resonance concept of nucleon-nucleon and meson-nucleon interactions at low invariant energy $\sqrt{s}$ [22], adopting all resonance parameters from the Manley analysis [25]. The high energy collisions – above $\sqrt{s} = 2.6$ GeV for baryon-baryon collisions and $\sqrt{s} = 2.2$ GeV for meson-baryon collisions – are described by the LUND string fragmentation model FRITIOF [26]. This aspect is similar to that used in the HSD approach [6, 27, 28, 29] and the UrQMD code [5]. For a detailed description of the underlying model at low energy we refer the reader to Ref. [24].

For later discussions it is essential to realize that the code respects detailed balance only for reactions of the type $1 \leftrightarrow 2 + 3$ and approximately for $1 + 2 \leftrightarrow 3 + 4$ [1] where the numbers $1, \ldots, 4$ are any reaction partners. This implies that in particular at high energies, where the string degrees of freedom with their decay to many (> 2) final particles becomes important, detailed balance is violated. We will discuss the consequences of this violation, which is inherent in all such transport codes, at the appropriate points in the following sections.

2.1 A box with periodic boundary conditions

In order to study 'infinite' hadronic matter problems we confine the particles in a cubic box with periodic boundary conditions for their propagation similar to a recent box calculation within the UrQMD model [18]. We specify the initial conditions, i.e. baryon density ρ, strange particle density ρ_S and energy density ε as follows: first the initial system is fixed to $N_p = 80$ protons and $N_n = 80$ neutrons, which are randomly distributed in a cubic box of volume V. The 3-momenta $\vec{p}_i$ of the nucleons in a first step are randomly distributed inside a Fermi-sphere of radius $p_F = 0.26$ GeV/c (at ρ_0) and in a second step boosted by

---

[1]In the latter case small violations of detailed balance are due to the treatment of t-channel and background contributions.

$\pm\beta_{cm}$ by a proper Lorentz transformation. Thus the initial baryon density ρ is fixed as $\rho = A/V$, $A = N_p + N_n$. The strange particle density is set to zero as in related heavy-ion experiments while the energy density is defined as $\varepsilon = E/V$, where E is the total energy of all nucleons

$$E = \sum_i^A \sqrt{p_i^2 + m_N^2}. \tag{1}$$

The boost velocity β_{cm} is related to the initial energy density ε (excluding Fermi motion) as

$$\beta_{cm} = \sqrt{1 - \frac{\rho^2 m_N^2}{\varepsilon^2}} \tag{2}$$

using

$$\varepsilon = \gamma_{cm} \rho m_N \tag{3}$$

with $\gamma_{cm} = 1/\sqrt{1 - \beta_{cm}^2}$. Recall that $\rho_0 m_N \simeq 0.15$ GeV/fm^3 so that an energy density $\varepsilon \simeq 1.5$ GeV/fm^3 at density ρ_0 corresponds to $\gamma_{cm} \simeq 10$, i.e. the SPS energy $T_{lab} \simeq 185$ A·GeV. We thus start with a 'true' nonequilibrium situation in order to mimique the initial stage in a relativistic heavy-ion collision. The initial phase represents two interpenetrating, (ideally) infinitely extended fluids of cold nuclear matter.

We now propagate all particles in the box in the cascade mode (without mean-field potentials) using periodic boundary conditions, i.e. particles moving out of the box are reinserted at the opposite side with the same momentum. The phase-space distribution of particles then can change due to elastic collisions, resonance and string production and their decays to mesons and baryons again. We recall that we include all baryon resonances up to an invariant mass of 2 GeV and meson resonances up to the ϕ-meson. According to the initial conditions for ε and ρ the factor γ_{cm} in (3) determines if strings are excited in the very first collisions. This is the case for $\gamma_{cm} > 1.4$ where the early equilibration stages are dominated by string formation and decay.

2.2   Chemical equilibration

Figure 1 shows the time evolution of the various particle abundances (nucleons N, Δ, Λ, π, η, K^+ and K^- mesons) for density $\rho = \rho_0$ (left panel) at different energy densities $\varepsilon = 1.1, 0.52$ and 0.22 GeV/fm^3 and for $\rho = 3\rho_0$ (right panel) at $\varepsilon = 3.4, 1.57$ and 0.66 GeV/fm^3. These initial conditions correspond to bombarding energies T_{lab} per nucleon of roughly 100, 20 and 2 A·GeV, respectively. In Fig. 1 (as well as in Figs. 2,3) we count all particles which are 'hadronized', i.e. produced by string decay after a formation time of $\tau_F = 0.8$ fm/c in their rest frame.

After several fm/c the number of nucleons decreases due to inelastic collisions that produce either baryon resonances or additional mesons. The number of Δ-resonances grows up to a maximum in a few fm/c, since a lot of Δ's are produced in the first NN collisions; their number subsequently decreases with time due to their decay and excitation of further resonances or due to reabsorption. The numbers of π's and η's increase very fast and reach the equilibrium value within a few fm/c whereas the strange particles (K^+, K^-, Λ) require a much longer time for equilibration.

In Fig. 2 we present the time evolution of the particle ratios π/N, Δ/N, Λ/N, K^+/π^+, K^-/π^-, η/π for density $\rho = \rho_0$ at energy densities $\varepsilon = 1.1, 0.52$ and 0.2 GeV/fm^3, while Fig. 3 shows the same particle ratios for density $\rho = 3\rho_0$ at energy densities $\varepsilon = 3.4, 1.57$ and 0.66 GeV/fm^3, respectively. The left panels in both plots correspond to the full time scale as in Fig. 1 (up to 1000 fm/c), whereas the right panels present in more detail the initial phase (up to 30 fm/c). We use the same scale for the y-axis on the right and left panels, so one can easily see that the π/N, Δ/N ratios reach the equilibrium values very fast especially at low energy density since the string degrees of freedom here play a minor role and pion production basically emerges through Δ resonance decay.

The meson-pion ratios (K^+/π^+, K^-/π^-, η/π) at high energies show a decrease in the first few fm/c and then an increase again up to the equilibrium values. This is due to the fact that the bulk of the strange mesons is produced very early (at high energy density) through string formation and decay whereas most of the pions appear later, with a delay of several fm/c, as a result of the decay of heavy vector mesons (e.g. ρ and ω). From the right panels of Figs. 2 and 3 one can see that in the initial stage the particle ratios containing strange to nonstrange particles – K^+/π^+, K^-/π^-, Λ/N – are still far off chemical equilibrium for all energies and densities and the equilibration takes up to a few hundred fm/c depending on the energy and baryon density.

For the higher energies the initial particle production proceeds via the formation and decay of string excitations. This leads in particular to a very early onset of strange particles (mainly kaons and hyperons) within the first fm/c either due to the initial strings or due to secondary or ternary baryon-baryon, meson-baryon and meson-meson induced string-like interactions (see the right panels of Figs. 2 and 3). In Ref. [29] it was shown that these early secondary and ternary reactions can contribute up to about 50 % of the total strange particles obtained in a Pb + Pb reaction at CERN SPS energies and thus explain the factor of 2 in the observed relative strangeness enhancement compared to p+p reactions. This, however, does not imply that chemical equilibrium for the dominant strange particles has been achieved in this reaction, as our analysis clearly shows. In the later stages, when the system has become, more or less, isotropic in momentum space, strange particles can only be further produced by low energy hadronic reactions, which, however, have a considerable threshold and are thus strongly suppressed. This explains

the long chemical equilibration times for the strange particles first demonstrated by Koch, Müller and Rafelski [14].

In order to define an overall chemical equilibration time we perform a fit to the particle abundances $N(t)$ for pions and kaons as

$$N(t) = N_{eq} \left(1 - \exp(-t/\tau_{eq})\right), \tag{4}$$

where N_{eq} is the equilibrium limit. The equilibration time τ_{eq} thus corresponds to the time t when $\simeq 63\%$ of N_{eq} is achieved.

Figure 4 shows the equilibration time τ_{eq} versus energy density for π and K^+ mesons at different baryon densities of $1/3\rho_0, \rho_0, 3\rho_0$ and $6\rho_0$. We find that the equilibration time for pions scales as $\tau_{eq}^\pi \sim 1/\rho$ or $\Gamma_\pi \sim \rho$, thus we present the curve only for baryon density ρ_0. Whereas τ_{eq}^π slowly grows with energy-density, τ_{eq}^K falls steeply with ε. This marked difference is due to the fact that, on one hand, the kaon production rate increases dramatically with $\sqrt{s}$ whereas that of the pions, on the other hand, is more flat. With increasing energy thus more strange particles are produced through strings especially from the primary collisions with high $\sqrt{s}$ and the chemical equilibration is achieved faster.

In Fig. 4 we have considered an 'ideal' situation, i.e. hadron matter at fixed energy and baryon density. In realistic heavy-ion collisions the system goes through the different stages due to interactions and expansion. However, as follows from Fig. 4, the equilibration time for strangeness is larger than 40 fm/c for all energy and baryon densities. Thus in realistic nucleus-nucleus collisions the chemical equilibration of strange particles requires also a time above 40 fm/c which is considerably larger than the actual reaction time of a few 10 fm/c or less (cf. Section 4).

The particle abundances used to extract τ_{eq} in Fig. 4 have been calculated without any in-medium potentials. In fact, the introduction of attractive potentials (especially for K^-) will lower the hadronic thresholds and thus increase the scattering rate between strange and nonstrange hadrons, whereas the K^+ feels some repulsive potential and the trend goes in the opposite way. According to our calculations such in-medium modifications (in line with Ref. [6]) give a correction to the K^+ equilibration times by atmost 10 % and shortens the K^- equilibration times up to 20 % at density ρ_0.

2.3   Thermal equilibration and limiting temperature

In this subsection we investigate the approach to thermal equilibration. This is initially driven by the very early string phase on the momentum equilibration of the hadronic degrees of freedom, when the system is still very far from equilibrium and the energy density is sufficiently high. This one can see by looking at the quadrupole moment $<Q_2> = < 2p_z^2 - p_x^2 - p_y^2 >$ of the momentum distribution of all hadrons involved. In the left panel of Fig. 5 we present the time evolution of the quadrupole moment $< Q_2 >$

for density $\rho = \rho_0$ at energy densities $\varepsilon = 0.22$, 0.3, 0.52, 0.8, 1.1 and 1.6 GeV/fm^3. In order to take into account the string contributions we have counted here all particles even within the formation time. The thin solid lines indicate exponential fits of the form

$$< Q_2 > (t) \simeq A_1 \exp(-t/\tau_{short}) + A_2 \exp(-t/\tau_{long}) \tag{5}$$

with two equilibration times τ_{short} and τ_{long}.

The right panel of Fig. 5 shows τ_{short} and τ_{long} versus energy density ε. Whereas $\tau_{short} \simeq 5$ fm/c is roughly independent on ε the 'hadronic' equilibration time τ_{long} increases with energy density. These results have to be interpreted as follows: in the initial nonequilibrium phase the string degrees of freedom are excited and decay according to many-body phase on a short time scale τ_{short}. The string decays reduce the initial quadrupole moment (at high energy density) in time by a significant factor of about $3 - 4$. One can understand the result obtained for τ_{short} in a rather simple way. Due to our prescription of the initialization of the system the first strings on average are formed after the time $\tau_{coll} \approx 1/((\rho/2)\sigma_{NN}\langle v_{NN}\rangle) \approx 3 - 4$ fm/c for $\rho = \rho_0$. The strings then decay within their formation time $\tau_F \approx 0.8$ fm/c giving rise to a significant production of transversal momentum. One should point out, that according to these arguments τ_{short} approximately scales like $1/\rho$. Due to Lorentz contraction τ_{short} is thus considerably smaller in a real heavy-ion collision. Hence, string decays provide a very efficient source for a strong decrease in longitudinal momentum and production of transverse momentum in the very early stage of an ultrarelativistic heavy-ion collision. A decrease (increase) of the formation time τ_F to 0.5 fm/c (1.5 fm/c) changes τ_{short} on the scale of 20%, only.

After string decay, however, the emerging hadronic system still has significantly larger longitudinal than transverse momenta – the ratio increases with energy density ε – and low energy hadronic reactions are less effective in transfering longitudinal to transverse momentum or simply in production of mesons. This explains the increase of τ_{long} with ε in simple terms.

From the above analysis it follows that after typical relaxation times of $\tau_{short} \approx 5$ fm/c the momentum unisotropy of hot and dense matter has dropped to e^{-1} such that one might describe the system by simple global thermodynamical variables like temperature etc. This thermal equilibrium has to be contrasted with the chemical equilibrium which – as we have shown in the preceding subsection – is reached only after much longer times (≥ 40 fm/c for strange particles, for example).

For the equilibrated system we can extract a temperature T by fitting the particle spectra with the Bolzmann distribution

$$\frac{d^3 N_i}{dp^3} \sim \exp(-E_i/T), \tag{6}$$

where $E_i = \sqrt{p_i^2 + m_i^2}$ is the energy of particle i. We note that at the temperatures of

interest here, the Bose and Fermi distributions are practically identical to a Boltzmann distribution. We find that in equilibrium the spectra of all particles can be characterized by one single temperature T. This is demonstrated in Fig. 6 where we show the spectra of nucleons (N), pions (π) and kaons (K^+) as a function of the kinetic energy $E - m$ for $\rho = \rho_0$ at energy densities $\varepsilon = 0.52, 0.8$ and 1.6 GeV/fm^3 (left panel) and for $\rho = 3\rho_0$ at energy densities $\varepsilon = 0.66, 1.57$ and 2.85 GeV/fm^3 (right panel). Here we have averaged the spectra from 950 fm/c to 1000 fm/c in order to decrease the numerical fluctuations. The spectra of N, π, K^+ here can be fitted with a single temperature T which increases with the energy density ε for both baryon densities ρ_0 and $3\rho_0$. We note explicitly that the slope of the equilibrium particle spectra does not depend on the formation time τ_F.

In Fig. 7 we display the energy density ε versus temperature T for different baryon densities ρ: $1/3\rho_0$ (open down triangles), ρ_0 (full squares), $3\rho_0$ (full dots), $6\rho_0$ (full up triangles). In order to compare calculations for different baryon densities we have subtracted the baryon energy density at rest, i.e. $\simeq m_N\rho$ (except for Fermi motion). As seen from Fig. 7 the temperature grows with energy density up to a limiting value reminiscent of a 'Hagedorn' temperature [30]. From our detailed investigations we obtain for the limiting temperature $T_s \simeq 150 \pm 5$ MeV which practically does not depend on baryon density. Such a singular behavior of $\varepsilon(T)$ for $T \simeq T_s$ has also been found in the box calculations in Ref. [18] for $\rho = \rho_0$. Our limiting temperature is slightly higher than that in Ref. [18] ($T_s = 130 \pm 10$ MeV) due to the different number of degrees of freedom; the model [18] contains more resonances and uses a different threshold for string excitations. Thus, there is some phenomenological sensitivity to the hadronic zoo of particles and string thresholds employed in the model.

In Fig. 8 we show the excitation function for the ratio of string energy density to the energy density of the whole system $\varepsilon_{string}/\varepsilon$ at $\rho = \rho_0$ when the system has equilibrated for long times. If the equilibrated system is very dense, lower energy strings are still continuously being excited and thus – because of their subsequent decay – the strings constitute a stationary portion of the total energy of the system. The relative ratio in the energy density increases with ε up to a saturation value of $\simeq 16\%$ and then stays essentially constant. This reflects that the system reaches a limiting temperature, since the relative amount of string excitations compared to resonance excitations does not change any more, whereas the number of strings as well as the number of hadrons produced increases with ε. This fact one might have guessed since the string production rate in equilibrium depends only on the temperature T characterizing the Bose/Fermi distributions in the collision terms. In addition, this constant fraction, of course, also intrinsically depends on the excitation threshold and on the chosen decay (or formation) time τ_F of the strings.

As pointed out above, the string degrees of freedom play an essential role for particle production at high bombarding energies since they describe the continuum excitations

of the system. The number of strings created is especially high at the first stages of the collision, when the energy of baryon-baryon interactions is close to the initial energy $\sqrt{s}$. It decreases with time to some constant value which corresponds to the equilibrium state. Because of this string-dominance one now has to worry about possible consequences of a violation of detailed balance for these degrees of freedom. As already pointed out earlier, all hadronic cascade-type approaches use the phenomenological string picture in order to describe quantitatively energetic (soft or semi-hard) inelastic reactions above some specified $\sqrt{s}$-threshold. In such binary hadronic reactions typically many hadronic particles and resonances are produced, the number depending on the incident energy $\sqrt{s}$. The 'back reaction' of these particles produced from decay of an excited string (or two strings in the LUND model) leading to the formation of only two energetic hadrons again is not considered as it is statistically suppressed and difficult to describe. On the other hand, in an 'infinite' matter calculation these back reactions have to be taken into account in order to allow for the principle of detailed balance. This is not done here as it is technically difficult to handle; it thus represents a potential 'Achilles heal' in a thermodynamic analysis. However, for simulating a heavy-ion collision this deficiency is not of any major importance since the excitation of strings happens in the first moment of the reaction when the phase space is still widely open and no back reaction can occur.

2.4 Comparison to the statistical model

In order to investigate the equilibrium behavior of hadron matter we also compare our transport (box) calculations with a simple Statistical Model (SM) for an Ideal Hadron Gas (IHG) where the system is described by a grand canonical ensemble of non-interacting fermions and bosons in equilibrium at temperature T. All baryon and meson species considered in the transport model [23] also have been included in the statistical model. Our main objective here is to compare our results with the Hagedorn bootstrap picture of hadronic matter [30].

We recall that in the SM particle multiplicities n_i and energy densities ε_i are given by

$$n_i = \frac{g_i}{(2\pi\hbar)^3} \int_0^\infty \frac{4\pi p^2 dp}{\exp\left[(E_i - B_i\mu_B - S_i\mu_S)/T\right] \pm 1}, \tag{7}$$

$$\varepsilon_i = \frac{g_i}{(2\pi\hbar)^3} \int_0^\infty \frac{4\pi E_i p^2 dp}{\exp\left[(E_i - B_i\mu_B - S_i\mu_S)/T\right] \pm 1}, \tag{8}$$

where $E_i = \sqrt{p^2 + m_i^2}$ is the energy of particle i, B_i is the baryon charge, S_i is the strangeness, and g_i is the spin-isospin degeneracy factor. In Eqs. (7),(8) μ_B and μ_S are the baryon and strangeness chemical potentials. Here we neglect the electric chemical potential ($\mu_n = \mu_p = \mu_B$) since we consider an isospin symmetric system. Note, however,

that in realistic collisions of heavy-ions (like Au + Au) this reduction is no longer fully appropriate. For particles with finite spectral width we include in Eqs. (7),(8) the spectral functions $\rho_i(m)$ with the same parametrization for the width as in the transport model,

$$n_i = \frac{g_i}{(2\pi\hbar)^3} \int \rho_i(m)dm \int_0^\infty \frac{4\pi p^2 dp}{\exp\left[(E_i - B_i\mu_B - S_i\mu_S)/T\right] \pm 1}, \tag{9}$$

$$\varepsilon_i = \frac{g_i}{(2\pi\hbar)^3} \int \rho_i(m)dm \int_0^\infty \frac{4\pi E_i p^2 dp}{\exp\left[(E_i - B_i\mu_B - S_i\mu_S)/T\right] \pm 1}. \tag{10}$$

The energy density ε, baryon density ρ and strange density of the hole system in equilibrium then given as

$$\varepsilon = \sum_i \varepsilon_i(T, \mu_B, \mu_S) \tag{11}$$

$$\rho = \sum_i B_i \, n_i(T, \mu_B, \mu_S) \tag{12}$$

$$\rho_S = \sum_i S_i \, n_i(T, \mu_B, \mu_S) \equiv 0. \tag{13}$$

As 'input' for the SM we use the same ε, ρ and ρ_S as in the box calculations and we obtain the thermodynamical parameters – T, μ_B, μ_S – by solving the system of nonlinear equations (11),(12) and (13).

Within the SM we find that the temperature increases continuously with energy density since the continuum excitations, i.e. the string degrees of freedom, are not included (full dots in Fig. 9), whereas the box calculation with strings gives the limiting temperature (full squares in Fig. 9). Both curves in Fig. 9 have been calculated for density ρ_0.

To reproduce qualitatively our box result within the SM we have to include continuum excitations in the statistical model, i.e. a Hagedorn mass spectrum for strings as defined by [30]

$$\rho^{str}(m) = \frac{\rho_0^{str}}{m^3} \exp(m/T_H), \tag{14}$$

where T_H denotes the 'Hagedorn' temperature. For T_H we use the temperature T_s as obtained from the box calculations, i.e. $T_H = T_s \simeq 150$ MeV. In (14) ρ_0^{str} is a fit parameter additionally to T, μ_B and μ_S to reproduce $\varepsilon(T)$ from the box calculations. The string multiplicities n_i^{str} are given by

$$n_i^{str} = \frac{1}{(2\pi\hbar)^3} \int_{m_{min}}^\infty \rho_i^{str}(m)dm \int_0^\infty \frac{4\pi p^2 dp}{\exp\left[(E_i - B_i\mu_B - S_i\mu_S)/T\right] \pm 1}, \tag{15}$$

where the lowest mass in the string excitation (m_{min}) is defined by the string threshold in the transport model: $m_{min} = 2.6 - m_N$ GeV for baryon strings and $m_{min} = 2.2$ GeV for meson strings. In our transport model we include the following strings i: baryon strings

$B = 1, S = 0, -1, -2, -3$, anti-baryon strings $B = -1, S = 0, 1, 2, 3$, meson strings $B = 0, S = 0, 1$ and anti-meson strings $B = 0, S = -1$.

Before going over to the actual analysis we point out that the limiting temperature T_s from our string model involves somewhat different physics assumptions than the Hagedorn model at temperature T_H. T_s should not really be identified with the 'Hagedorn' temperature T_H, though close similarities exist. In the Hagedorn picture and for temperatures close to T_H the abundance of 'normal' hadrons or known resonances stays constant with increasing energy density whereas the number and energy density of the (hypothetical) bootstrap excitations diverges for $T \to T_H$. The Hagedorn model thus assumes 'particles' of mass $m \to \infty$ to be populated for $T \to T_H$, that dynamically can be formed in collisions of high mass hadrons for $t \to \infty$. In contrast, our string model does not include energetic string-string interactions that might produce more massive strings. (There exist some phenomenological recipes how to incorporate such interactions [31].) The 'high mass' strings decay to hadrons and, because of the detailed balance problem discussed in the last subsection, are only repopulated by binary hadron-hadron or hadron-string interactions, so that their internal energy is limited and the low-energy hadronic degrees of freedom are overpopulated. This leads to the saturation of string-energy to total energy (observed in Fig. 8) to a value of $\simeq 0.16$ in contrast to the value of 1 in the Hagedorn model.

This, however, does not imply a fundamental inconsistency for the overall properties of the system. In perfect chemical equilibrium, like in the Hagedorn model, more strings (or hypothetical resonances) would be excited which, for lower temperatures (e.g. in a nearly isentropic expansion of the system like in heavy-ion collisions), would immediately decay into a large number of hadronic particles. The violation of detailed balance in our case thus physically describes an overpopulation of hadronic particles only in stationary equilibrium. The important point, however, is the observation that in either description the system at equilibrium can not exceed the critical temperature T_s.

As seen in Fig. 9 we achieve agreement of the extended SM and our box calculations from Fig. 8 by choosing $T_H \approx T_s$ in Eq. (14). In addition, from the extended SM we can also define thermodynamical parameters such as the baryon chemical potential μ_B. In Fig. 10 we present the resulting $T - \mu_B$ correlation, i.e. temperature T versus baryon chemical potential μ_B, at fixed baryon densities (in the box calculations) of $\rho = 1/3\rho_0, \rho_0$ and various energy densities. The open triangles and squares (connected by the dashed lines) show the result of the SM without strings at densities $1/3\rho_0$ and ρ_0, respectively, whereas the full triangles and squares (connected by the solid lines) correspond to the thermodynamical fit of the box calculations (at $1/3\rho_0$ and ρ_0) including string excitations. The errorbars indicate the uncertainty in the extraction of μ_B in the SM; they become larger when the system is closer to T_H due to the divergence in the energy density integral

(11). The arrow at $\mu_B = 0$ indicates the temperature $T_s = 150$ MeV from our box calculations. The full dots in Fig. 10 correspond to chemical freeze-out points extracted in a thermodynamical model from hadron abundances [7]; the open dots are the thermal freeze-out points from the momentum spectra of hadrons and two-particle correlations as taken from Ref. [32].

Our calculations here are for nuclear matter densities $1/3\rho_0$ and ρ_0 whereas the freeze-out points have been extracted from heavy-ion data; the comparison thus can be only qualitative. However, one can see the general tendency: if the continuum excitations (strings) are not included in the thermodynamical analysis, one can 'extract' much larger temperatures at high energy density simply due to the limited number of degrees of freedom involved in the model analysis. In this respect our box result is more in line with the thermal ('kinetic') freeze-out analysis from Ref. [32] than with the thermodynamical analysis from Ref. [7] that is based on particle ratios and thus on chemical freeze-out. The point to make is that at higher temperatures, like e.g. the ones obtained for a 'chemical' freeze-out in Ref. [7], the consideration of continuum excitations does make a thermodynamical analysis much less certain than at lower temperatures, like e.g. at 'thermal' (or kinetic) freeze-out as in Ref. [32], where the continuum excitations do not play any significant role.

In this context we have to mention, furthermore, that a combined experimental analysis of particle spectra and HBT radii favors even lower freeze-out temperatures (below 100 MeV [33, 34]). For these freeze-out conditions the pion density (for fixed charge) drops below $\sim 10^{-2}$ fm^3, i.e. the average distance between two pions (of different charge) becomes large than ~ 4.6 fm, which in turn is large compared to their classical interaction radius $r_I = \sqrt{\sigma_{\pi\pi}/\pi}$ at all relative momenta between the two pions. Since thermal freeze-out temperatures of 90-100 MeV at SPS energies can be considered as a lower bound, the 'experimental' points in Fig. 10 have to be taken with care.

3 Expanding hadronic fireballs

In realistic nucleus-nucleus collisions the system rapidly expands after the possible formation of a hot hadronic fireball. The final hadronic spectra can be changed substantially during this expansion phase, i.e. the temperature extracted from the experimentally observed slopes of the spectra also contains information about the nuclear expansion dynamics.

To investigate the expansion of the hadronic fireball we initialize the system in a box with periodic boundary conditions – as described above – and propagate the system up to 500 fm/c, when equilibrium is reached. Afterwards we let the system expand without boundary conditions. Even though this is an idealized description of the expansion phase

during a heavy-ion collision we hope to learn from this scenario how the expansion stage changes the picture of perfect thermal equilibrium (for an analysis of an actual collision see the discussion in the following section).

In Fig. 11 we present the time evolution of the various particle abundances (nucleons N, Δ, Λ, π, K^+ and K^- mesons) during the expansion for density $\rho = \rho_0$ (left panel) at different energy densities $\varepsilon = 0.22, 0.3$ and 1.1 GeV/fm^3 and for density $\rho = 1/3\rho_0$ at $\varepsilon = 0.84$ GeV/fm^3 (upper part in the right panel), for $\rho = \rho_0$ at $\varepsilon = 1.6$ GeV/fm^3 (middle part in the right panel) and for $\rho = 3\rho_0$ at $\varepsilon = 3.4$ GeV/fm^3 (lower part in the right panel). The number of stable particles ($N, \Lambda, \pi, K^+, K^-$) increases during the expansion up to some asymptotic value due to string and heavy resonance decay as well as inelastic interactions. One can see that the asymptotic values are reached after a few 10 fm/c from the beginning of the expansion (depending on the initial energies and baryon densities) which is comparable to the actual reaction time in heavy-ion collisions (cf. Section 4).

In Fig. 12 we show the spectra of nucleons (N), pions (π) and kaons (K^+) versus the kinetic energy $E - m$ for $\rho = \rho_0$ at energy densities $\varepsilon = 0.22, 0.3$ and 1.1 GeV/fm^3 before the expansion – averaged over time from 450 fm/c to 500 fm/c – (left panel) and after the expansion – averaged from 580 fm/c to 600 fm/c – (right panel). For completeness in Fig. 13 we present the result for $\rho = 1/3\rho_0$ at $\varepsilon = 0.84$ GeV/fm^3 (upper part), for $\rho = \rho_0$ at $\varepsilon = 1.6$ GeV/fm^3 (middle part) and for $\rho = 3\rho_0$ at $\varepsilon = 3.4$ GeV/fm^3 (lower part). In the left panels the systems are in equilibrium; the N, π, K^+ spectra show a common temperature T whereas after the expansion the slopes of the particle spectra are different; the nucleon spectra are much harder than the pion spectra, i.e. the apparent temperature of particles (after the expansion) increases with the mass m. This effect is illustrated in Fig. 14, where we show the apparent slope T versus m for π, K^+, N for $\rho = \rho_0$ at different energy densities: $\varepsilon = 0.2$ GeV/fm^3 (full up triangles), $\varepsilon = 0.3$ GeV/fm^3 (full squares), $\varepsilon = 1.1$ GeV/fm^3 (full dots), $\varepsilon = 1.6$ GeV/fm^3 (full diamonds); and for $\rho = 3\rho_0$ at $\varepsilon = 3.4$ GeV/fm^3 (open down triangles). The arrow indicates the limiting temperature $T_s = 150$ MeV before the expansion. One can see from Figs. 12–14 that the 'expansion' temperature of particles increases also with the energy density. However, if during the equilibration phase the system reaches T_s, the 'expansion' temperatures for different particles show a universal behaviour, i.e. practically do not depend on the energy ε as well as on the baryon density ρ. This phenomenon is due to the fact that close to T_s the initial hadron velocity distributions, reflected in the particle momentum profile, become similar for all ε and ρ in equilibrium.

In order to investigate the origin of the enhancement in the particle slope during the expansion we have performed several illustrative calculations: at 500 fm/c – after the system has achieved equilibrium – we i) let all resonances and strings decay; in this case we find that the slopes do not change as compared to the equilibrium phase, ii) we let

13

the system expand without interactions (allowing only decays) and find that the slopes slightly decrease in comparison to the equilibrium phase. Both examples indicate that the slope enhancement stems basically from multiple interactions of the particles in the initial stages of the expansion phase.

For analyzing the expansion flow phenomena we have performed a fit of the particle spectra (after expansion) using the blast model of Siemens and Rasmussen [35]. In this model all particle spectra are described by a universal formula with common thermal freeze-out parameters, i.e. a temperature T of the fireball and a radial-flow velocity β:

$$\frac{d^3 N_i}{dp^3} = A_i \exp\left(-\frac{\gamma E_i}{T}\right) \left[\frac{\sinh \alpha_i}{\alpha_i}\left(\gamma + \frac{T}{E_i}\right) - \frac{T}{E_i} \cosh \alpha_i\right], \tag{16}$$

where $\gamma = (1 - \beta^2)^{-1/2}$, $\alpha = \gamma \beta p_i / T$. Here E_i, p_i are the total energy and momentum of the considered particle i while A_i are normalization factors.

We now try to describe the final particle spectra after the expansion by Eq. (16) with common freeze-out parameters T and β. In Fig. 15 we show the result of our least-squares fit, using the MINUIT method [36], for the energy densities $\varepsilon = 0.3$ GeV/fm^3 (upper part) and 1.1 GeV/fm^3 (lower part) at $\rho = \rho_0$. The left panel shows the contour plots for the parameter errors in the $T - \beta$ plane (for the $\chi^2_{optimal} + 1$ level); the dot-dashed lines stand for nucleons (N), the solid lines for pions (π) and the dashed lines for kaons (K^+). The full symbols indicate the 'best' values for T and β according to the χ^2 criteria (squares for N, dots for π and triangles for K^+). The thin solid lines in the right panel demonstrate the fit of the particle spectra within the optimal parameters from MINUIT.

Since the particle spectra cover several orders of magnitude and the low energy points contribute to χ^2 with a larger weight than those at high energy, we use the logarithmic χ^2 method to give a higher weight to the tail of the spectra in the fitting procedure, i.e. we minimize $\chi^2_{\ln} = \sum_i (\ln f(x_i) - \ln f_0(x_i))^2$, where f_0 represent the 'experimental' data (i.e. the results of our box calculations), f is the value of the fit (16) at point x_i.

One can see from Fig. 15 that the 'best' parameters T and β (as well as the contours for the parameter errors) are quite different for N, π and K^+ especially for $\varepsilon = 0.3$ GeV/fm^3. So we do not find (within the 'optimal' χ^2) common freeze-out parameters for all spectra simultaneously. This is similar to an analysis of experimental spectra by Peitzmann et al. [37]. For all particles we obtain different values for β and much lower temperatures T than that of the initial fireball: $T_{in} = 107$ MeV for $\varepsilon = 0.3$ GeV/fm^3 and $T_{in} = 145$ MeV for $\varepsilon = 1.1$ GeV/fm^3.

Since especially the pion spectra contain large contributions from resonance decays at low $E - m$, we have also performed fits excluding the pion spectra for $E - m \leq 0.4$ GeV. This procedure essentially gives lower β parameters and higher values for T (open circle in the upper panel). However, the low energy cut-off is an additional parameter that allows to 'extend' the (β, T) values to a wider range.

Thus our analysis indicates that the final particle spectra do not allow a reliable reconstruction of freeze-out parameters within the collective flow model (16). The parameters T and β obtained from the fit are very sensitive to the low energy shape of the hadron spectra or low energy cut-off applied since this region contributes with the largest weight to the χ^2 minimization. On the other hand, a global 'eye' fit with the parameters given by the 'star' for all hadrons considered gives a quite reasonable overall description of the spectra (dashed lines, r.h.s of Fig. 15), too. A very accurate deduction of one single overall fit for all hadrons by a common temperature (T) and flow velocity (β) parameter (see, e.g., [32] and references therein) seems to us thus rather ambiguous. In particular, such an analysis may indicate that thermal equilibrium has been reached to a much larger extent than is actually true.

The particle flow effect due to the expansion is demonstrated in Fig. 16 where we show the velocity distributions $dN/d\beta$ for nucleons (N), pions (π) and kaons (K^+) for $\rho = 1/3\rho_0$ at $\varepsilon = 0.84$ GeV/fm^3 (upper part), for $\rho = \rho_0$ at $\varepsilon = 1.1$ GeV/fm^3 (middle part) and for $\rho = 3\rho_0$ at $\varepsilon = 3.4$ GeV/fm^3 (lower part). The left panel shows the $dN/d\beta$ distribution at equilibrium whereas the right panel corresponds to $dN/d\beta$ after the expansion phase. On can see that the average velocity of the particles decreases with the mass; the pions are much faster than the nucleons. They thus leave the reaction zone at the initial stage of the ongoing and rapidly evolving expansion with a higher velocity and accelerate the slower hadrons that 'feel' the 'pion wind' by the multiple interactions [38]. We recall that the pion density is very high especially at high ε such that practically all other hadrons are shifted in direction of large β. The same effect is shown in Figs. 12,13 by the enhancement of the slope of the nucleon spectra due to the expansion.

4   Reactions of finite systems

In this Section we turn to realistic nucleus-nucleus collisions with the BUU transport model. We have learned from our analysis in the previous Section that even by starting from an idealized scenario of perfect thermal equilibrium, a rapid expansion stage makes the extraction of one global temperature T and one global expansion parameter β quite ambiguous. We thus expect this to become even worse for the true situation of a relativistic heavy-ion collision, where a perfect equilibrium state at some intermediate stage cannot really be assumed. Also, we note that even for a very heavy system like Pb+Pb the fraction of effective surface layer ($\sim 4\pi R_{eff}^2 \lambda$) to total volume is still quite sizeable, resulting in a continuous emission or evaporation of particles from the outer layers before a global freeze-out of bulk particles occurs. (For Pb+Pb reactions at SPS energies – combining a hydrodynamical evolution with a nonequilibrium picture of surface emission – it has indeed been shown that at least 25% of all particles are continuously evaporated

before a global freeze-out has occurred [40].)

In Fig. 17 we show the time evolution of the particle abundances (nucleons N, Δ, Λ, π, η, K^+) for central collision of the light system ^{12}C + ^{12}C (upper part) and heavy system ^{197}Au + ^{197}Au and ^{208}Pb + ^{208}Pb (lower part) at the low energy of 1 A·GeV (left panel) and the high energy of 100 and 160 A·GeV (right panel). The number of nucleons decreases in a few fm/c due to the inelastic collisions, whereas the number of Δ-resonances increases accordingly. At low energy the η-mesons and strange particles (we disregard strange particles for C + C at 1 A·GeV due to the low statistics) appear with a delay of a few fm/c due to the fact that they are basically produced from resonance decays (the same as pions) or from secondary pion-baryon collisions, whereas at high energy they appear earlier due to the primary production mechanism through the string formation and decay.

As seen from Fig 17 the reaction time τ_{reac} for 1 A·GeV is $\sim 20 - 30$ fm/c, whereas for high energies τ_{reac} is shorter due to a faster expansion – $\tau_{reac} \simeq 10 - 20$ fm/c. It has been shown in Section 2.2 that the chemical equilibration of hadronic matter under 'ideal' conditions (box without expansion) requires a quite long time, e.g. the equilibration time τ_{eq} for strange particles has been found to be larger than 40 fm/c for all energies and densities (cf. Fig. 4). In realistic central nucleus-nucleus collisions, such as Au + Au, the system expands rapidly (depending on the energy) after the compression and formation of the hadronic fireball. The number of interactions, which is the dynamical origin for equilibration, decreases correspondingly very fast with time; after a few 10 fm/c the particles are moving practically freely. Thus, the reaction time even for central Au + Au collisions is much shorter than the time required for strangeness equilibration: $\tau_{reac} \ll \tau_{eq}$.

The thermal equilibration time in this energy range around 0.25 GeV/fm^3, as obtained from the box calculation, is about 5–7 fm/c (see Fig. 5). Notice, however, that this calculation – because of its periodic boundary conditions – probably underestimates the equilibration time. Indeed, studies of the longitudinal and transverse temperatures (T_L and T_T, resp.) [16, 24] have shown that full thermal equilibrium is reached only in the very late expansion phase, when the density ρ has dropped already below its saturation value. After a period of 10 fm/c (after first contact) one still finds $T_L \approx 1.5\,T_T$, i.e. an anisotropy of about 40 %, considerably more than indicated in Fig. 5. At the bombarding energy of 160 A·GeV we find a rapid decrease of the quadrupole moment in the momentum space of all hadrons by about a factor of 3 at the scale of 5 fm/c leading to longitudinally expanding matter. In view of Fig. 5 this stretched ellipsoid in momentum space becomes isotropic only on the scale of 10–20 fm/c since low energy hadronic reactions are less effective for equilibration. Since this 'hadronic' equilibration time is larger than the reaction time for Pb + Pb at 160 A·GeV a substantial anisotropy remains in the hadron momentum distributions after the collision.

Contrary to the box case the d^3N/dp^3 spectra for realistic nucleus-nucleus collisions do not follow the simple exponential behaviour (6) due to the strong longitudinal expansion; especially at high bombarding energy the particle spectra show the specific 'banana' shape (reflecting the pp spectra at high energies). In order to exclude this simple dynamical effect related to the longitudinal expansion, we present in Fig. 18 (right panel) the transverse mass spectra $1/m_T^2 dN/dm_T$ at mid-rapidity ($-0.5 \leq y_{cm} \leq 0.5$) versus $m_T - m$ for central Au + Au collisions at 1 A·GeV (upper part) and for central Pb + Pb at 160 A·GeV (lower part) calculated at the end of the reaction. The m_T-spectra show an exponential behaviour [39] (excluding small m_T), however, with different slopes which can not be associated directly with a temperature of a hot fireball formed at the intermediate stages of the reaction.

In line with Section 3 we have performed a fit within the blast model (16) within an interval of unit rapidity around midrapidity using MINUIT. The results of the fit are displayed in Fig. 18. The full symbols (squares for N, dots for π and triangles for K^+) correspond to the 'best' values for T and β according to the χ^2 criteria. The thin solid lines in the right panel demonstrate the fit of the m_T spectra within the optimal fit parameters (we obtain a smaller χ^2 within the linear χ^2 method ($\chi^2 = \sum_i (f(x_i) - f_0(x_i))^2$), which provides a better description of the low m_T spectra).

Similar to Section 3 (cf. Fig. 15) we obtain (within the 'optimal' χ^2 criterium) quite different freeze-out parameters for N, π and K^+ spectra. In order to exclude the influence of Δ- (and other resonance) decays on the pion spectra and to investigate the sensitivity of the freeze-out parameters to the low energy cuts applied, we performed a fit of the particle spectra using the following cut-offs: $m_T - m > 0.2$ GeV (open symbols) and $m_T - m > 0.4$ GeV (open symbols with crosses inside) for Au + Au at 1 A·GeV; $m_T - m > 0.4$ GeV (open symbols) and $m_T - m > 0.5$ GeV (open symbols with crosses inside) for Pb + Pb at 160 A·GeV. As seen from the left panel of Fig. 18 the implementation of the low m_T cut-off leads to a substantial shift of the 'optimal' MINUIT parameters β and T especially for pions. The β, T values for the different spectra move towards to each other when discarding the low m_T points. For Au + Au at 1 A·GeV our β and T parameters agree with those extracted by the TAPS collaboration [41] using the blast model (star in the upper left plot). Here we have to mention that the cut-off $m_T - m > 0.4$ GeV has been applied in the experimental analysis, too [41]. For the Pb + Pb spectra at 160 A·GeV our freeze-out parameters are similar to those from Kämpfer [42] ($T = 120$ MeV, $\beta = 0.43$; star in the lower left plot). The dashed lines in the right panel of Fig. 18 show the fit to the particle m_T spectra for the β, T values corresponding to the 'stars' from the left panel. Again this 'eye' fit gives a reasonable description of the spectra (except of the very low m_T part).

Here we have to mention again that the extraction of freeze-out parameters from the

17

experimental data is very sensitive to the details of the thermodynamical model applied as well as to the observables considered. For example, the analysis of SIS data at 1.0 GeV from Ref. [11] gives thermal freeze-out parameters – $T \simeq 52$ MeV and $\beta \simeq 0.4$. At SPS energies the chemical freeze-out temperature extracted in Ref. [43] from the thermal-analysis of particle ratios is $T \simeq 168$ MeV, whereas the analysis of particle spectra and two-particle correlations (HBT data) [33, 34] provides a much lower thermal freeze-out temperature $T \simeq 90 - 95$ MeV. For a survey different freeze-out parameters the reader is referred to Fig. 4 of Ref. [44]).

In view of the various uncertainties inherent in the extraction of the thermal freeze-out parameters we conclude that a full, i.e. thermal and chemical, thermodynamical equilibrium at freeze-out cannot be deduced from such an analysis.

5   Summary

In this paper we have performed a systematic study of equilibration phenomena and equilibrium properties of 'infinite' hadronic matter as well as of relativistic nucleus-nucleus collisions using a BUU transport model that contains resonance and string degrees-of-freedom. The 'infinite' hadron matter is modelled by initializing the system at fixed baryon density, strange density and energy density by confining it in a cubic box with periodic boundary conditions.

We have shown that the equilibration times τ_{eq} for different particles depend on baryon density and energy density. The time τ_{eq} for non-strange particles is much shorter than for particles including strangeness; for kaons and antikaons the equilibration time is found to be larger than $\simeq 40$ fm/c for all baryon and energy densities considered. The overall abundance of the dominant strange particles (kaons and Λ's) being produced and obtained within the BUU cascade model for heavy-ion collisions can therefore not be described by assuming a perfect chemical equilibrium as strangeness is typically still undersaturated to a quite large extent. We mention taht transport model calculations like ours can describe the yield and spectra of the produced nonstrange hadrons as well as K^+, K^-, Λ yields quite well at SPS energies [6, 29]. On the other hand, at AGS energies the measured K^+/π^+ ratio in central Au + Au collisions is underestimated by about 30% [45]. However, we have to point out that the more exotic strange particles (like the measured antihyperon yields of Ref. [46]) can by far not be explained within such standard hadronic multiple channel reactions. These hadronic data possibly point towards new physics.

We have, furthermore, shown that thermal equilibrium is established quickly, within about 5 fm/c at SIS energies and samewhat larger times at high energies. The inclusion of continuum excitations, i.e. hadron 'strings', leads to a limiting temperature of $T_s \simeq$ 150 MeV in our transport approach which practically does not depend on the baryon

density and energy. We have compared our results with the statistical model (SM), which contains the same degrees of freedom and the same spectral functions of particles as our transport model. We found that the limiting temperature behaviour can be reproduced in the statistical model only after including continuum excitations of the Hagedorn type, otherwise the fireball temperature extracted from the particle abundances and spectra is overestimated substantially.

Close to the critical temperature T_s, the hadronic energy densities can increase to a couple of GeV/fm^3. From lattice QCD calculations one expects that a phase transition to a potentially deconfined QGP state should occur. Referring to the limiting temperature $T_s \approx 150$ MeV obtained, a QGP should be revealed and clearly distinguished from a hadronic state of matter if one can unambiguously prove the existence of an equilibrated and thermal phase of strongly interacting matter with temperatures exceeding, e.g., 200 MeV. The best candidates are electromagnetic probes, either direct photons or dileptons. On the other hand these are also 'contaminated' by hadronic background and/or pree-quilibrium physics. So far no thermal electromagnetic source with temperatures larger or equal than 200 MeV has been clearly identified.

We have also studied the expansion of the equilibrated hadronic fireball and found that the slope parameters of the particles after expansion increase with their mass; the pions leave the fireball much faster than nucleons and accelerate heavier hadrons by rescattering ('pion wind'). If the system before expansion is close to the limiting temperature T_s, the slope parameters for all particles after expansion practically do not depend on energy and baryon density. This is due to the fact that the particle velocity distributions in equilibrium do not change any more for $T \approx T_s$. We have fitted the resulting spectra within the blast model of Siemens and Rasmussen. Our analysis shows a strong sensitivity of the (β, T) parameters on the spectral shape at low energy (or a low energy cut-off) so that no reliable parameter determination can be reported. However, a global 'eye' fit with 'average' (β, T) parameters describes the data reasonably well.

Additionally, we have considered the equilibration in realistic nucleus-nucleus collisions of light (C + C) and heavy (Au + Au and Pb + Pb) systems. The (β, T) parameters extracted from our calculations for Au + Au at 1 A·GeV agree with those extracted from the TAPS collaboration [41] and for Pb + Pb at 160 A·GeV with the parameters from Ref. [42]. Here the reaction time is a few 10 fm/c and decreases with the initial energy due to the fast expansion. Since the reaction time is much shorter than the equilibration time for strangeness, a chemical equilibrium of strange particles in heavy-ion collisions is not supported by our transport calculations. Although again simple fits within the blast model provide a decent parametrization of our transport results for the differential particle spectra (Fig. 18) a deduction of global parameters for thermal freeze-out is again found to be rather ambiguous, especially when considering also the lower momentum contributions

of the various particle spectra.

Acknowledgements

References

[1] QUARK MATTER '96, Nucl. Phys. A 610 (1997) 1; QUARK MATTER '97, Nucl. Phys. A 638 (1998) 1; QUARK MATTER '99, Nucl. Phys. A (1999), in print.

[2] W. Botermans and R. Malfliet, Phys. Rep. 198 (1990) 115.

[3] P.A. Henning, Phys. Rep. 253 (1995) 235.

[4] G. Q. Li and C. M. Ko, J. Phys. G 22 (1997) 1673.

[5] S. A. Bass et al., Prog. Part. Nucl. Phys. 42 (1998) 279; J. Phys. G 25 (1999) 1859.

[6] W. Cassing and E. L. Bratkovskaya, Phys. Rep. 308 (1999) 65.

[7] P. Braun-Munzinger, J. Stachel, J.P. Wessels, and N. Xu, Phys. Lett. B 344 (1995) 43; P. Braun-Munzinger, J. Stachel, J.P. Wessels, and N. Xu, Phys. Lett. B 365 (1996) 1; J. Stachel, Nucl. Phys. A 654 (1999) 119.

[8] J. Cleymans and H. Satz, Z. Phys. C 57 (1993) 135.

[9] J. Sollfrank, M. Gazdzicki, U. Heinz and J. Rafelski, Z. Phys. C 61 (1994) 659; F. Becattini, M. Gazdzicki and J. Sollfrank, Eur. Phys. J. C 5 (1998) 143.

[10] C. Spieles, H. Stöcker and C. Greiner, Eur. Phys. J. C 2 (1998) 351.

[11] J. Cleymans, H. Oeschler, and K. Redlich, nucl-th/9809027; J. Phys. G 25 (1999) 281.

[12] H. Stöcker and W. Greiner, Phys. Rep. 137 (1986) 277.

[13] U. Ornik et al., Phys. Rev. C 54 (1996) 1381; S. Bernard et al., Nucl. Phys. A 605 (1996) 566; J. Sollfrank et al., Phys. Rev. C 55 (1997) 392.

[14] P. Koch, B. Müller, and J. Rafelski, Phys. Rep. 142 (1986) 167.

[15] W. Cassing, V. Metag, U. Mosel, and K. Niita, Phys. Rep. 188 (1990) 363.

[16] A. Lang, B. Blättel, W. Cassing, V. Koch, U. Mosel, and K. Weber, Z. Phys. A 340 (1991) 287.

[17] B. Blättel, V. Koch, and U. Mosel, Rep. Progr. Phys. 56 (1993) 1.

[18] M. Belkacem, M. Brandstetter, S.A. Bass et al., Phys. Rev. C 58 (1998) 1727.

[19] L.V. Bravina, M.I. Gorenstein, M. Belkacem et al., Phys. Lett. B 434 (1998) 379; L.V. Bravina, M. Brandstetter, M.I. Gorenstein et al., J. Phys. G 25 (1999) 351.

[20] L.V. Bravina, E.E. Zabrodin, M.I. Gorenstein et al., Phys. Rev. C 60 (1999) 024904.

[21] J. Sollfrank, U. Heinz, H. Sorge, N. Xu, Phys. Rev. C 59 (1999) 1637.

[22] S. Teis, W. Cassing, M. Effenberger, A. Hombach, U. Mosel, and Gy. Wolf, Z. Phys. A 356 (1997) 421.

[23] M. Effenberger, E.L. Bratkovskaya, and U. Mosel, Phys. Rev. C 60 (1999) 044614.

[24] M. Effenberger, Ph.D. Thesis, Univ. of Giessen, 1999; http://theorie.physik.uni-giessen.de/ftp.html.

[25] D. M. Manley and E. M. Saleski, Phys. Rev. D 45 (1992) 4002.

[26] B. Anderson, G. Gustafson and Hong Pi, Z. Phys. C 57 (1993) 485.

[27] W. Ehehalt and W. Cassing, Nucl. Phys. A 602 (1996) 449.

[28] E. L. Bratkovskaya and W. Cassing, Nucl. Phys. A 619 (1997) 413.

[29] J. Geiss, W. Cassing, and C. Greiner, Nucl. Phys. A 644 (1998) 107.

[30] R.Hagedorn, Suppl. Novo Cimento 3 (1965) 147; Suppl. Novo Cimento 6 (1965) 311; R.Hagedorn and J. Ranft, Suppl. Novo Cimento 6 (1968) 169.

[31] K. Sailer et al., J. Phys. G 17 (1991) 1005.

[32] U. Heinz, Nucl. Phys. A 638 (1998) 357c.

[33] J.R. Nix, Phys. Rev. C 58 (1998) 2303; J.R. Nix et al., nucl-th/9801045.

[34] B. Tomasik, U.A. Wiedemann and U. Heinz, nucl-th/9907096.

[35] P.J. Siemens and J.O. Rasmussen, Phys. Lett. 42 (1979) 880.

[36] F. James and M. Roos, Com. Phys. Commun. 10 (1975) 343.

[37] T. Peitzmann et al., Phys. Rev. Lett. 83 (1999) 926.

[38] M. Gyulassy, private communication.

[39] E.L. Bratkovskaya, W. Cassing and U. Mosel, Phys. Lett. B 424 (1998) 244.

[40] A. Dumitru, C. Spieles, H. Stöcker and C. Greiner, Phys. Rev. C56 (1997) 2202.

[41] R. Averbeck, nucl-ex/9803001.

[42] B. Kämpfer, J. Phys. G 23 (1997) 2001.

[43] P. Braun-Munzinger, I. Heppe and J. Stachel, Phys. Lett. B 465 (1999) 15.

[44] J. Cleymans and K. Redlich, Phys. Rev. C 60 (1999) 054908.

[45] W. Cassing, Nucl. Phys. A 661 (1999) 468c.

[46] E. Andersen et al. (WA97 Collaboration), Phys. Lett. B433 (1998) 209; J. Phys. G 25 (1999) 171; J. Phys. G 25 (1999) 181.
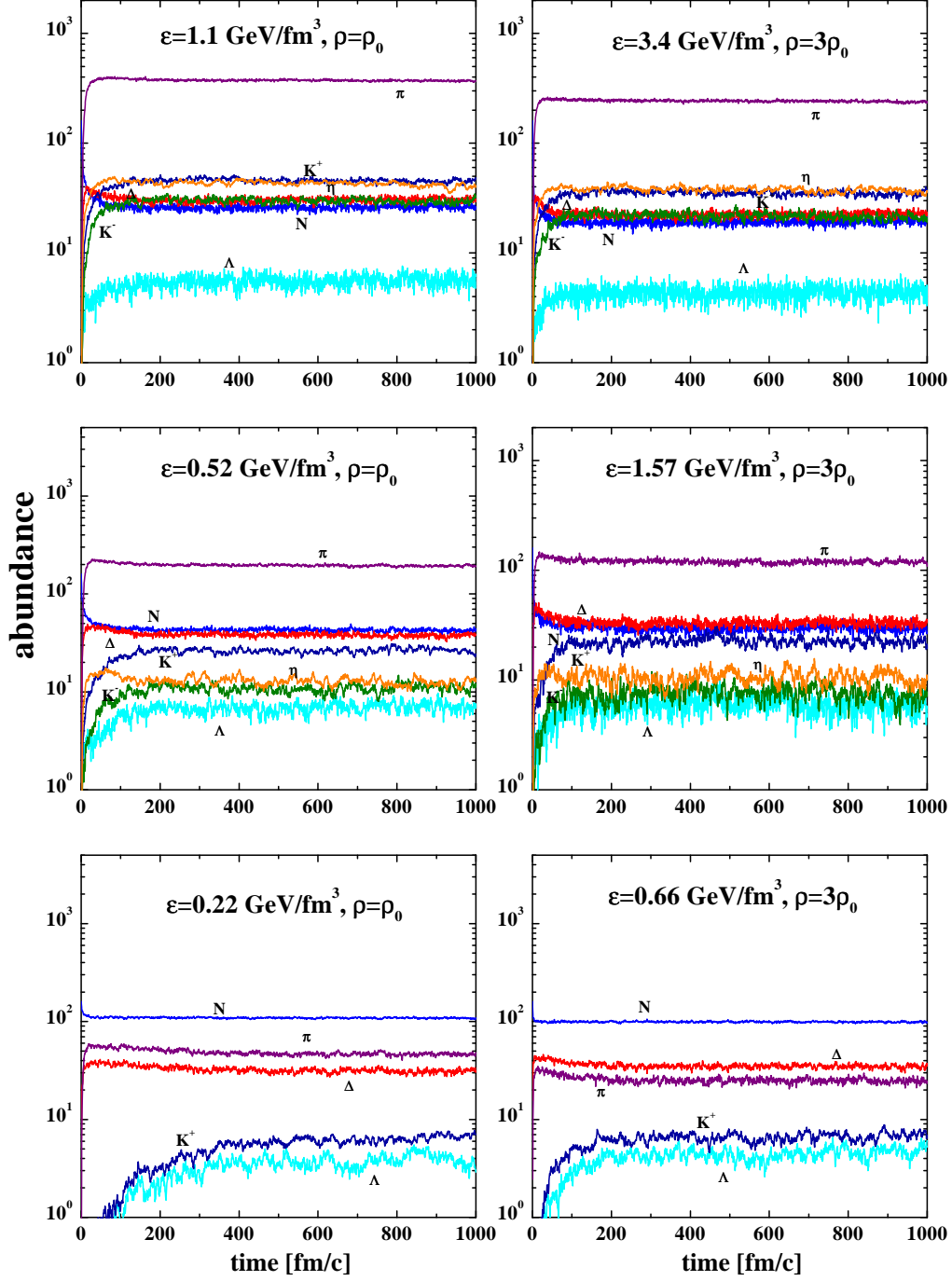
Figure 1: Time evolution of the various particle abundances (nucleons N, Δ, Λ, π, η, K^+ and K^- mesons) for density $\rho = \rho_0$ (left panel) at different energy densities $\varepsilon = 1.1, 0.52$ and 0.22 GeV/fm^3 and for $\rho = 3\rho_0$ (right panel) at $\varepsilon = 3.4, 1.57$ and 0.66 GeV/fm^3.
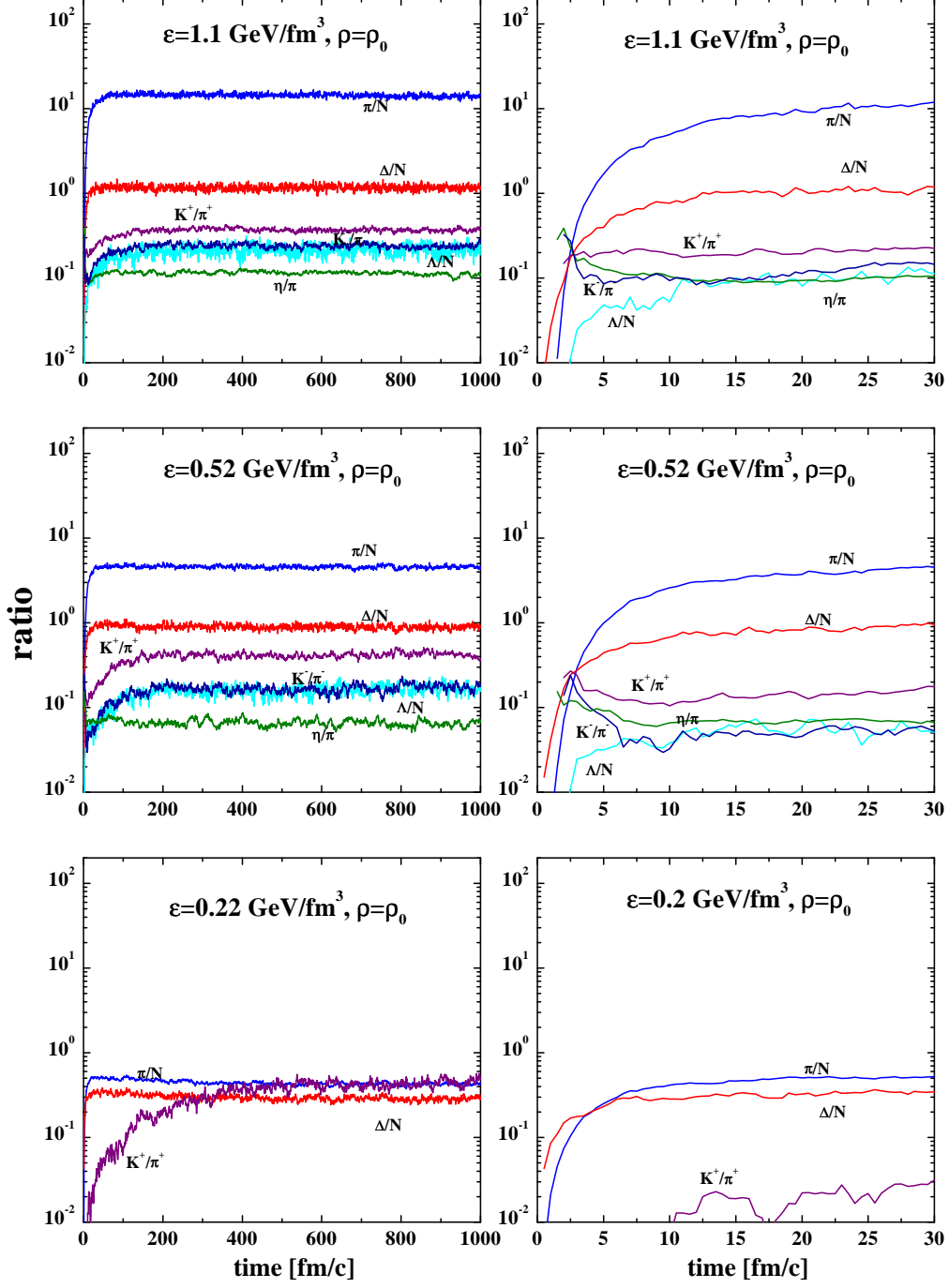
Figure 2: Time evolution of particle ratios π/N, Δ/N, Λ/N, K^+/π^+, K^-/π^-, η/π for density $\rho = \rho_0$ at energy densities $\varepsilon = 1.1, 0.52$ and 0.2 GeV/fm^3. The left panel shows the time scale up to 1000 fm/c, whereas the right panel demonstrates the initial stage up to 30 fm/c.

24
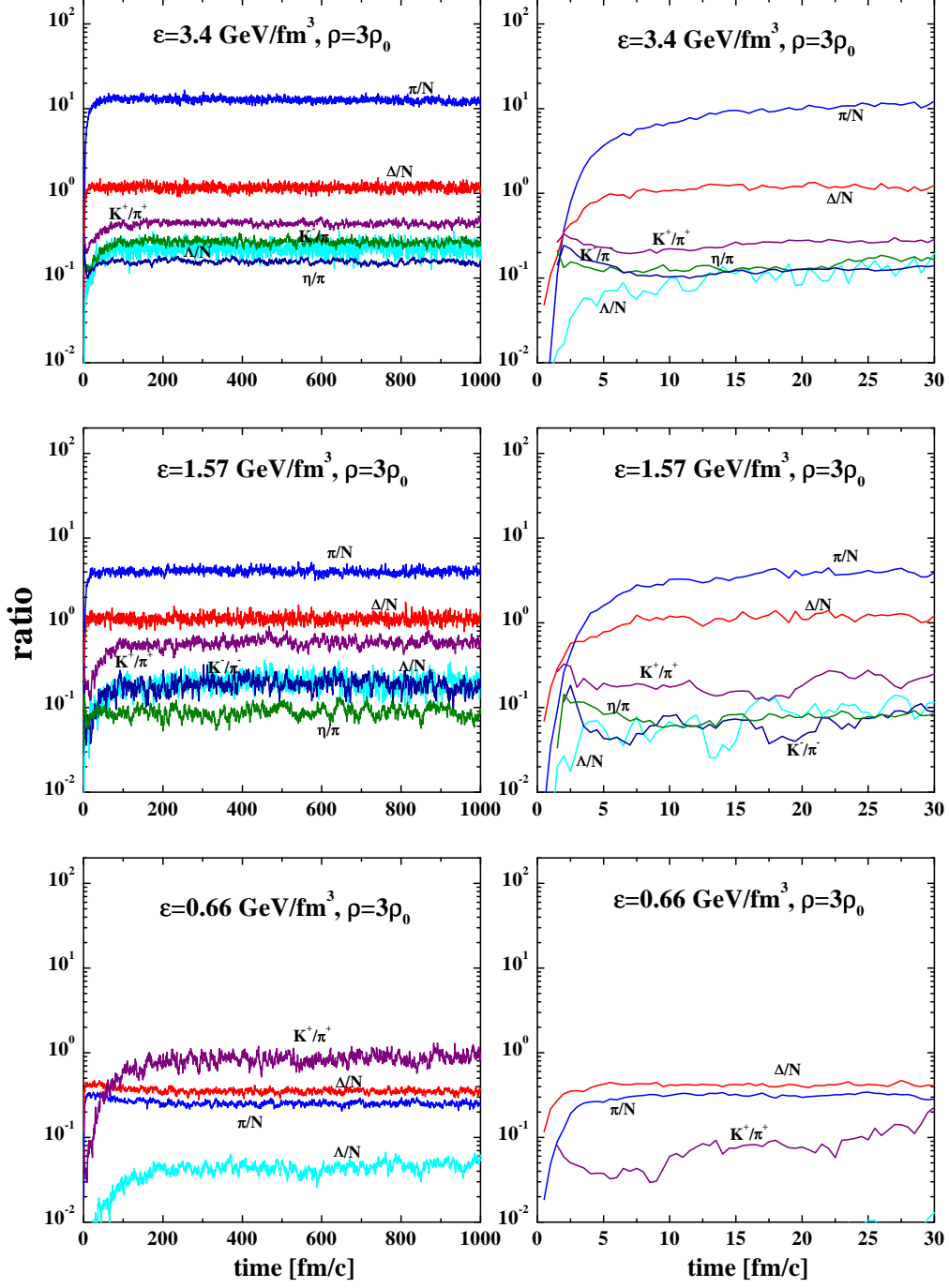
Figure 3: Time evolution of particle ratios π/N, Δ/N, Λ/N, K^+/π^+, K^-/π^-, η/π for density $\rho = 3\rho_0$ at energy densities $\varepsilon = 3.4, 1.57$ and 0.66 GeV/fm^3. The left panel shows the time scale up to 1000 fm/c, whereas the right panel demonstrates the initial stage up to 30 fm/c.

25
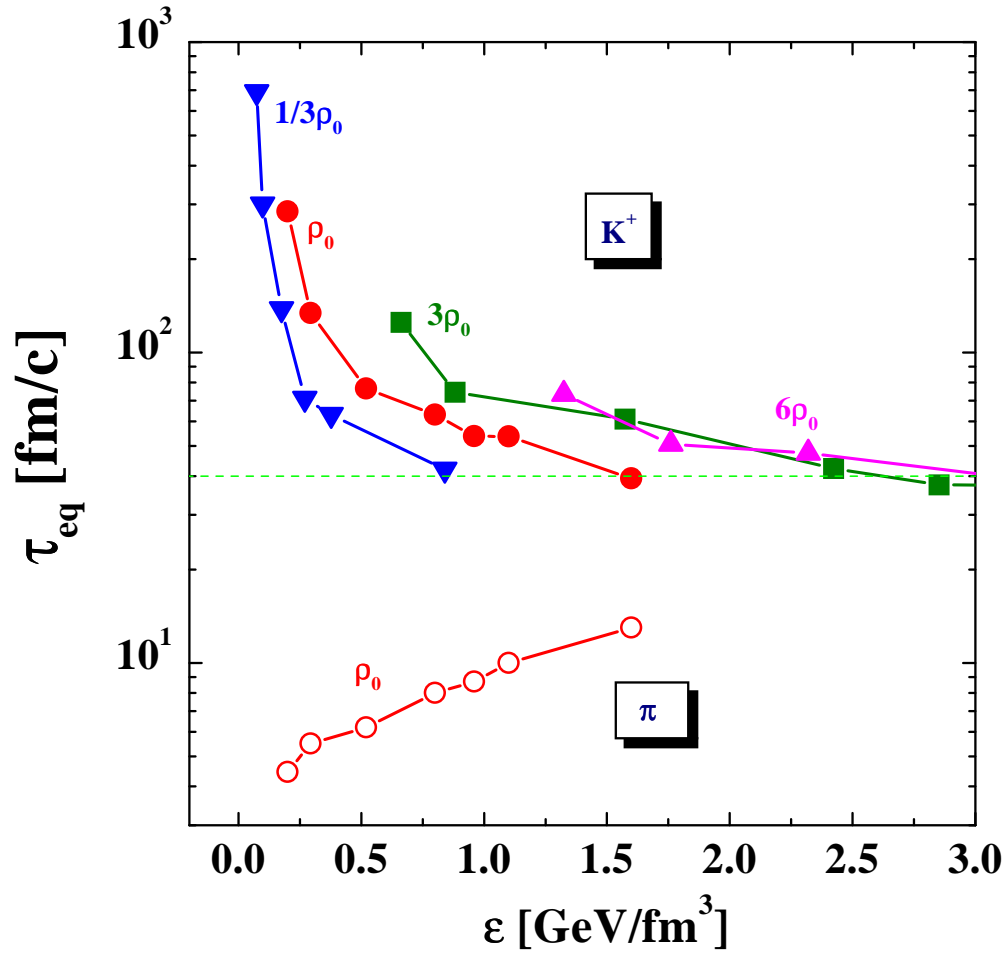
Figure 4: Equilibration time τ_{eq} versus energy density ε for π and K^+ mesons at different baryon densities $1/3\rho_0, \rho_0, 3\rho_0$ and $6\rho_0$.
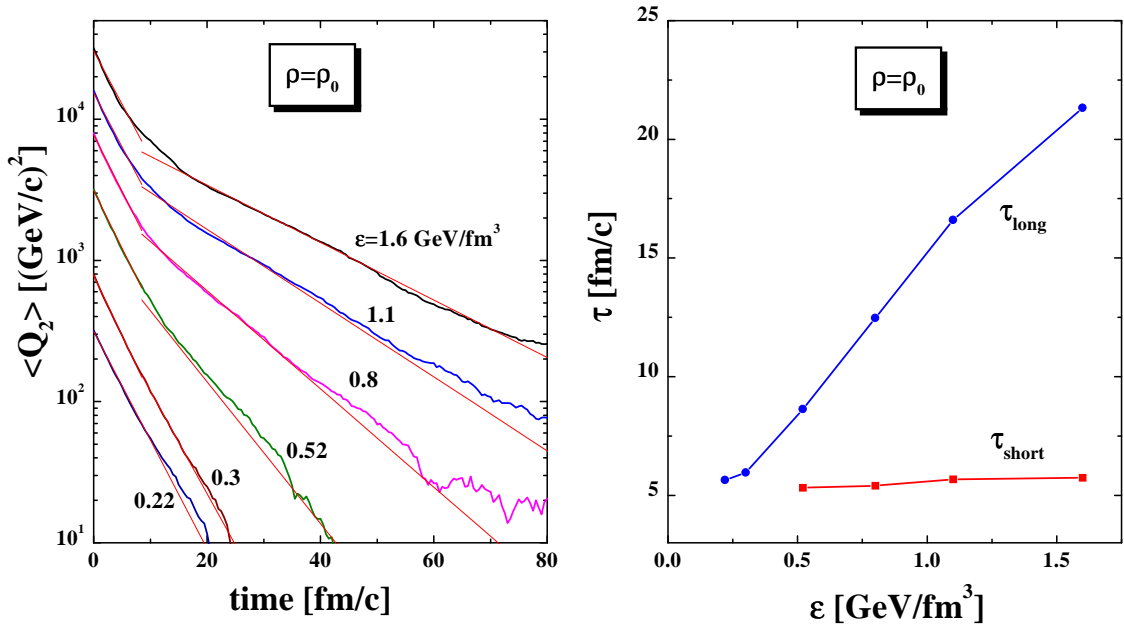
Figure 5: Left panel: time evolution of the quadrupole moment $< Q_2 >$ for density $\rho = \rho_0$ at energy densities $\varepsilon = 0.22, 0.3, 0.52, 0.8, 1.1$ and 1.6 GeV/fm^3. The thin solid lines indicate the fit of $< Q_2 >$ by two exponentials (5). The parameters τ_{short} and τ_{long} are shown in the right panel as a function of the energy density ε.
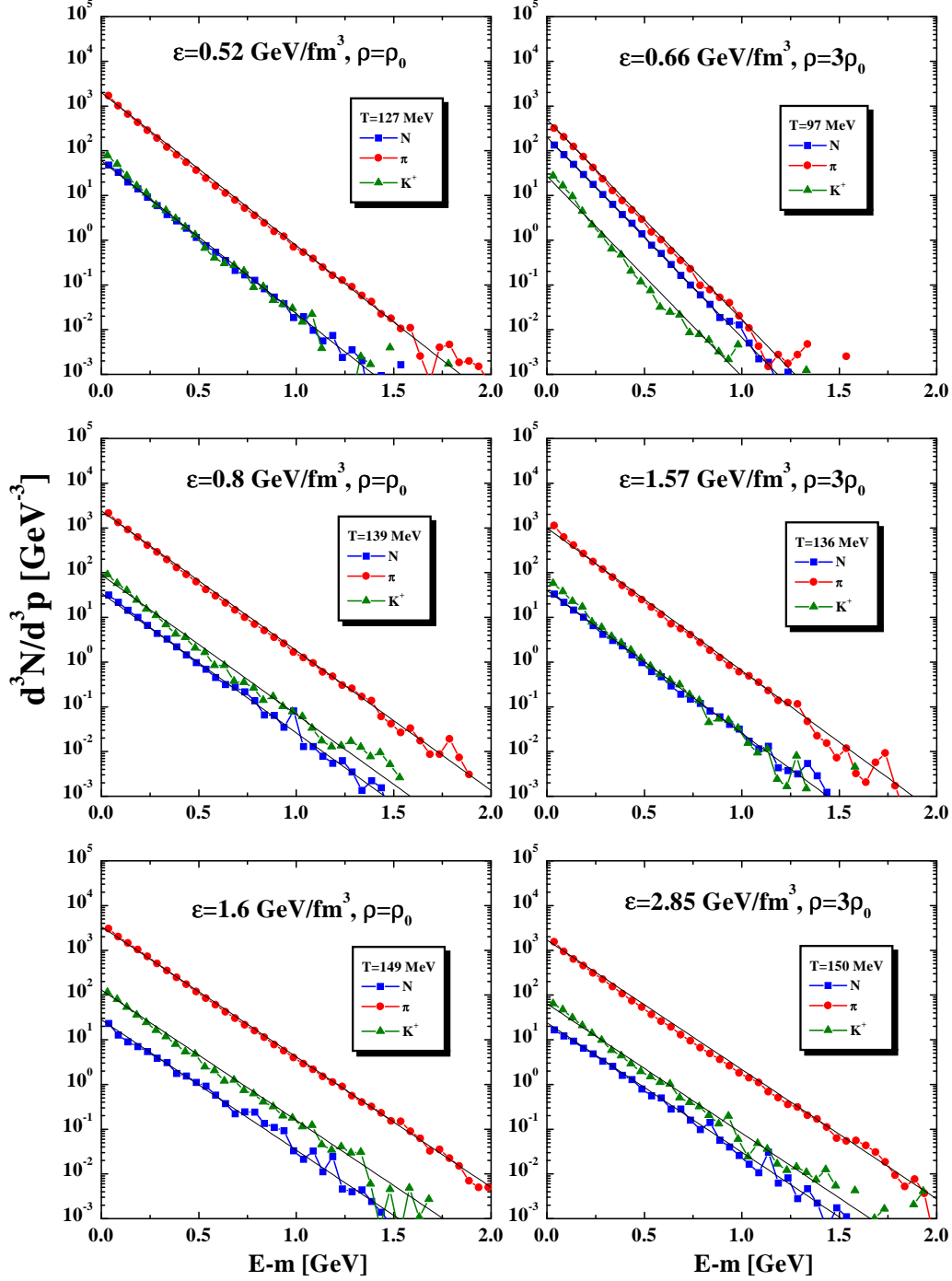
Figure 6: The spectra of nucleons (N), pions (π) and kaons (K^+) as a function of the kinetic energy $E - m$ for $\rho = \rho_0$ at energy densities $\varepsilon = 0.52, 0.8$ and 1.6 GeV/fm³ (left panel) and for $\rho = 3\rho_0$ at energy densities $\varepsilon = 0.66, 1.57$ and 2.85 GeV/fm³ (right panel).
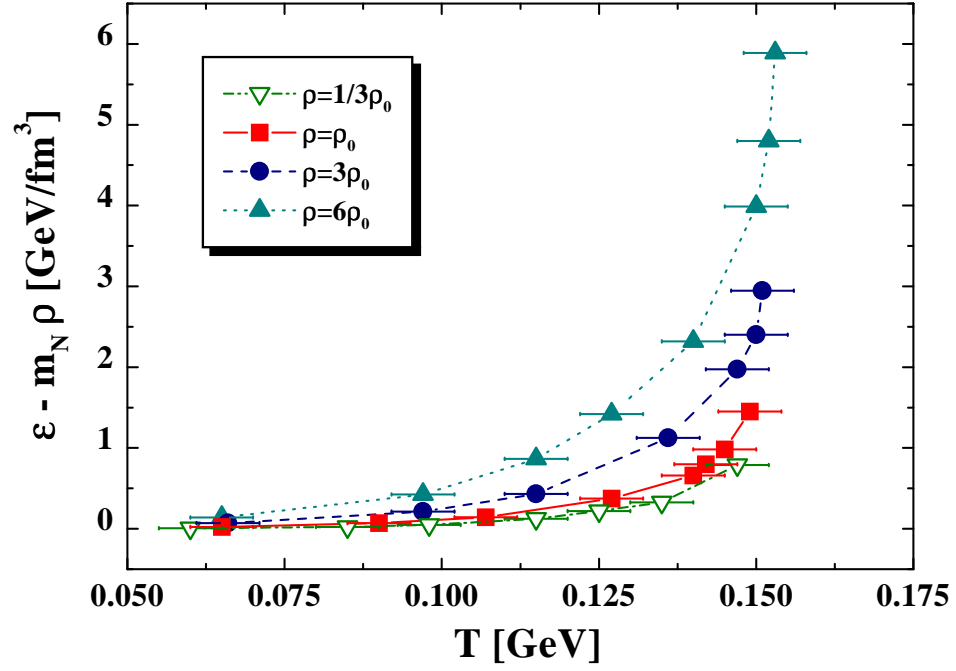
Figure 7: The energy density $\varepsilon - m_N\rho$ versus equilibrium temperature T for different baryon densities ρ: $1/3\rho_0$ (open down triangles), ρ_0 (full squares), $3\rho_0$ (full dots), $6\rho_0$ (full up triangles).
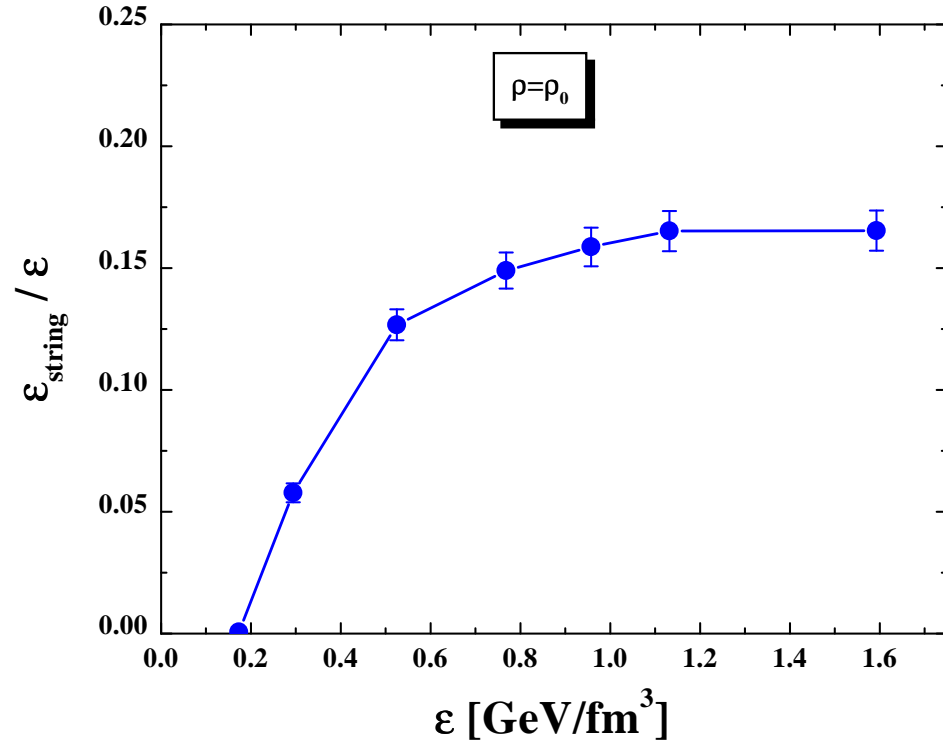
Figure 8: The excitation function for the ratio of string energy density to the energy density of the hole system $\varepsilon_{string}/\varepsilon$ at $\rho = \rho_0$.
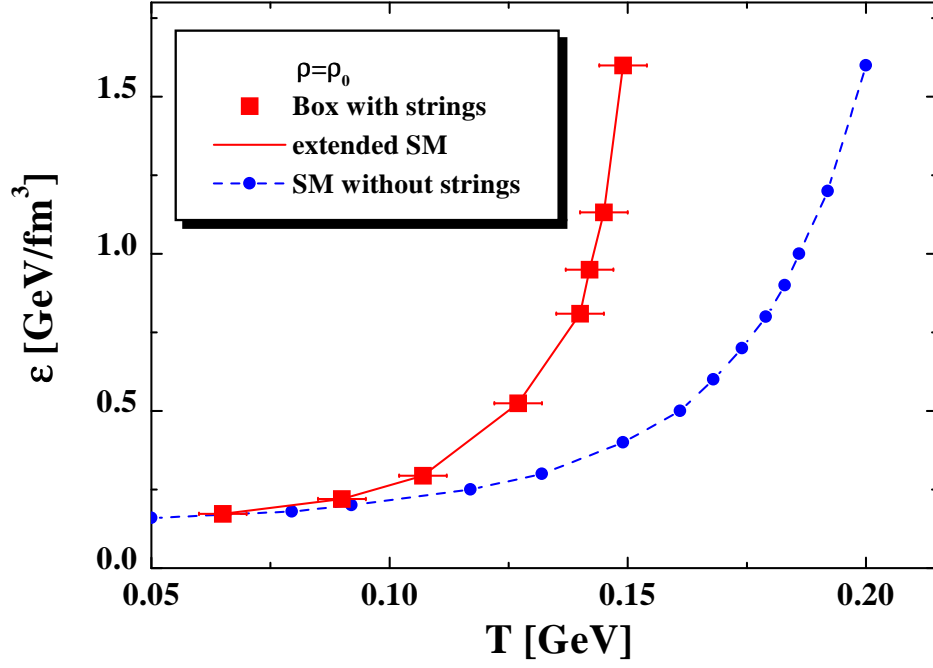
Figure 9: The energy density versus equilibrium temperature T for baryon density $\rho = \rho_0$. The full dots correspond to the statistical model (SM) without strings, the full squares show our box calculations including string degrees of freedom, while the solid line shows the result from the extended SM including a Hagedorn mass spectrum for strings.
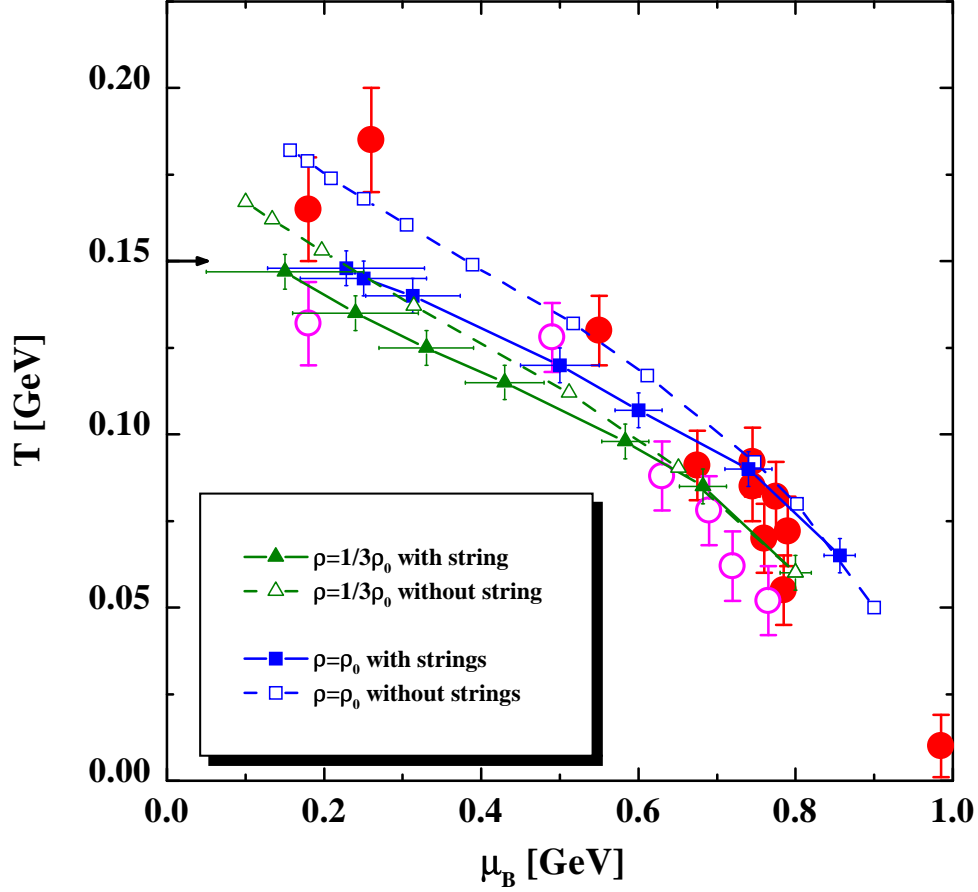
Figure 10: The $T - \mu_B$ phase correlation, i.e. temperature T versus baryon chemical potential μ_B. The open triangles and squares (connected by the dashed lines) show the result of the statistical model without strings (standard SM) fitted to out box calculations at densities $1/3\rho_0$ and ρ_0, respectively, whereas the full triangles and squares (connected by the solid lines) correspond to the thermodynamical fit of the box calculations (at $1/3\rho_0$ and ρ_0) including string excitations (extended SM). The arrow at $\mu_B = 0$ indicates the limiting temperature $T_s = 150$ MeV from our box calculations. The full dots correspond to the chemical freeze-out points from Ref. [7] while the open dots are the thermal freeze-out points from Ref. [32].
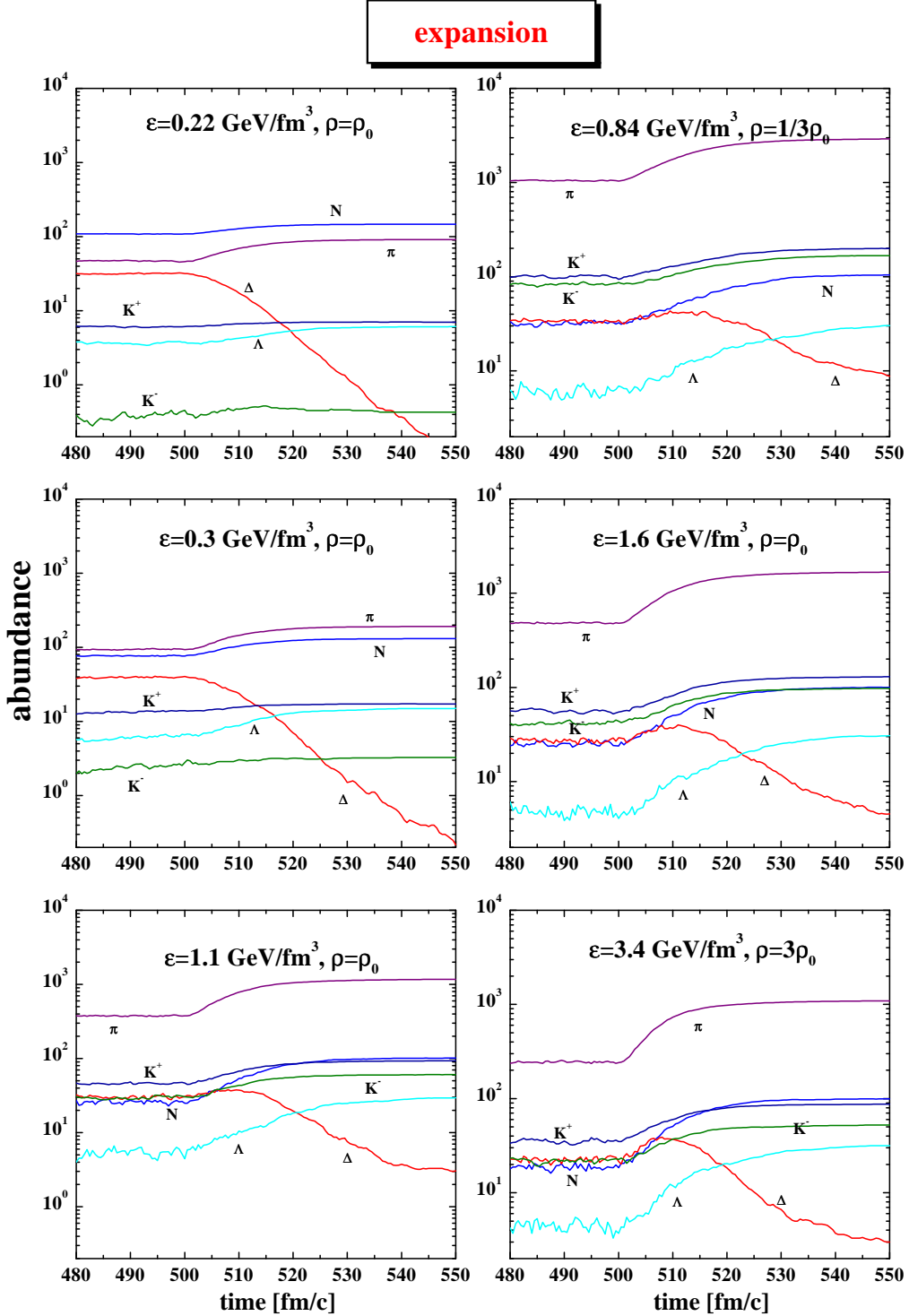
Figure 11: Time evolution of the various particle abundances (nucleons N, Δ, Λ, π, K^+ and K^- mesons) during the expansion (starting at $t = 500$ fm/c) for density $\rho = \rho_0$ (left panel) at different energy densities $\varepsilon = 0.22, 0.3$ and 1.1 GeV/fm³ and for density $\rho = 1/3\rho_0$ at $\varepsilon = 0.84$ GeV/fm³ (upper part in the right panel), for $\rho = \rho_0$ at $\varepsilon = 1.6$ GeV/fm³ (middle part in the right panel) and for $\rho = 3\rho_0$ at $\varepsilon = 3.4$ GeV/fm³ (lower part in the right panel).
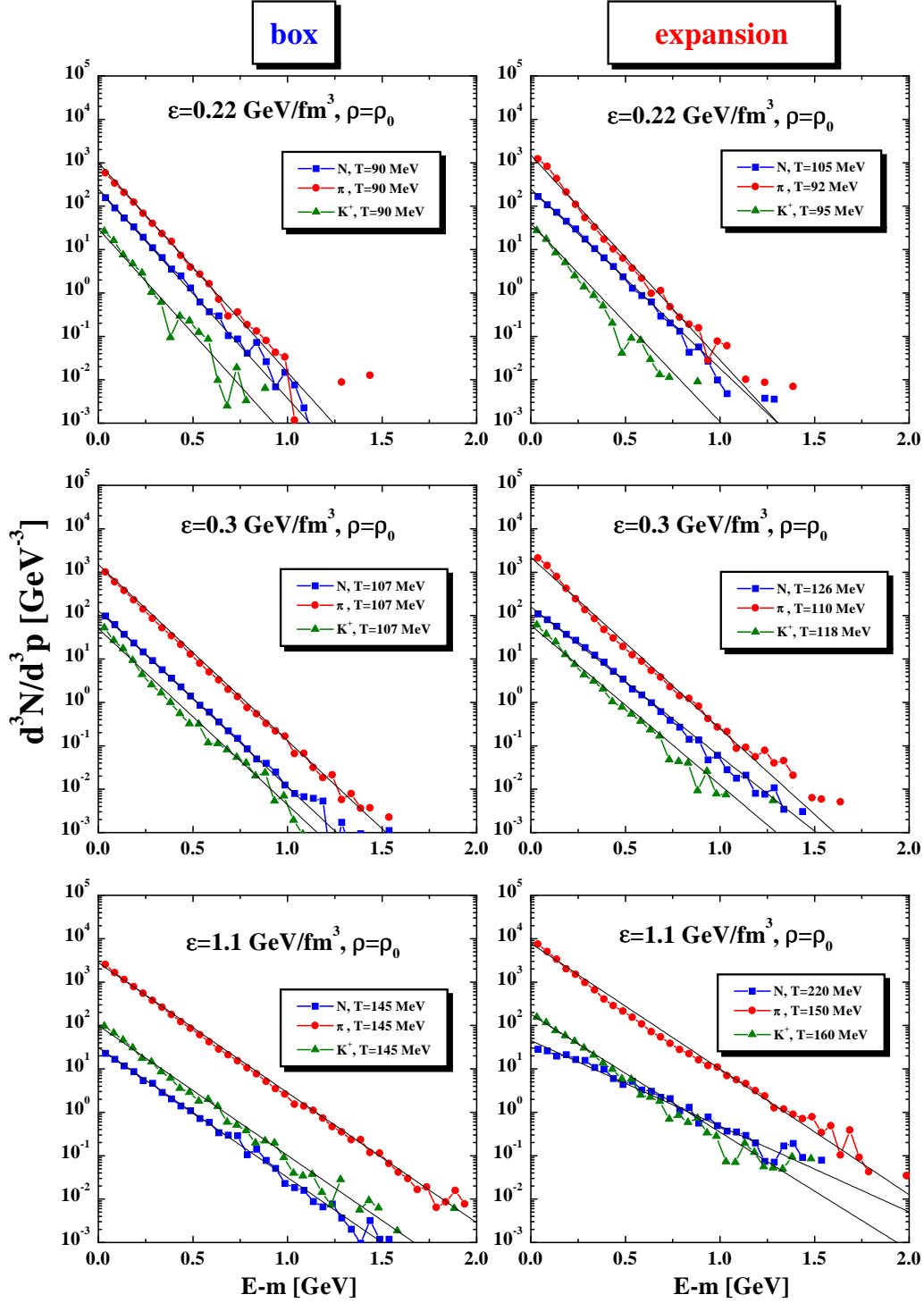
Figure 12: The spectra of nucleons (N), pions (π) and kaons (K^+) versus the kinetic energy $E - m$ for $\rho = \rho_0$ at $\varepsilon = 0.22, 0.3$ and 1.1 GeV/fm^3 before the expansion (left panel) and after the expansion (right panel).
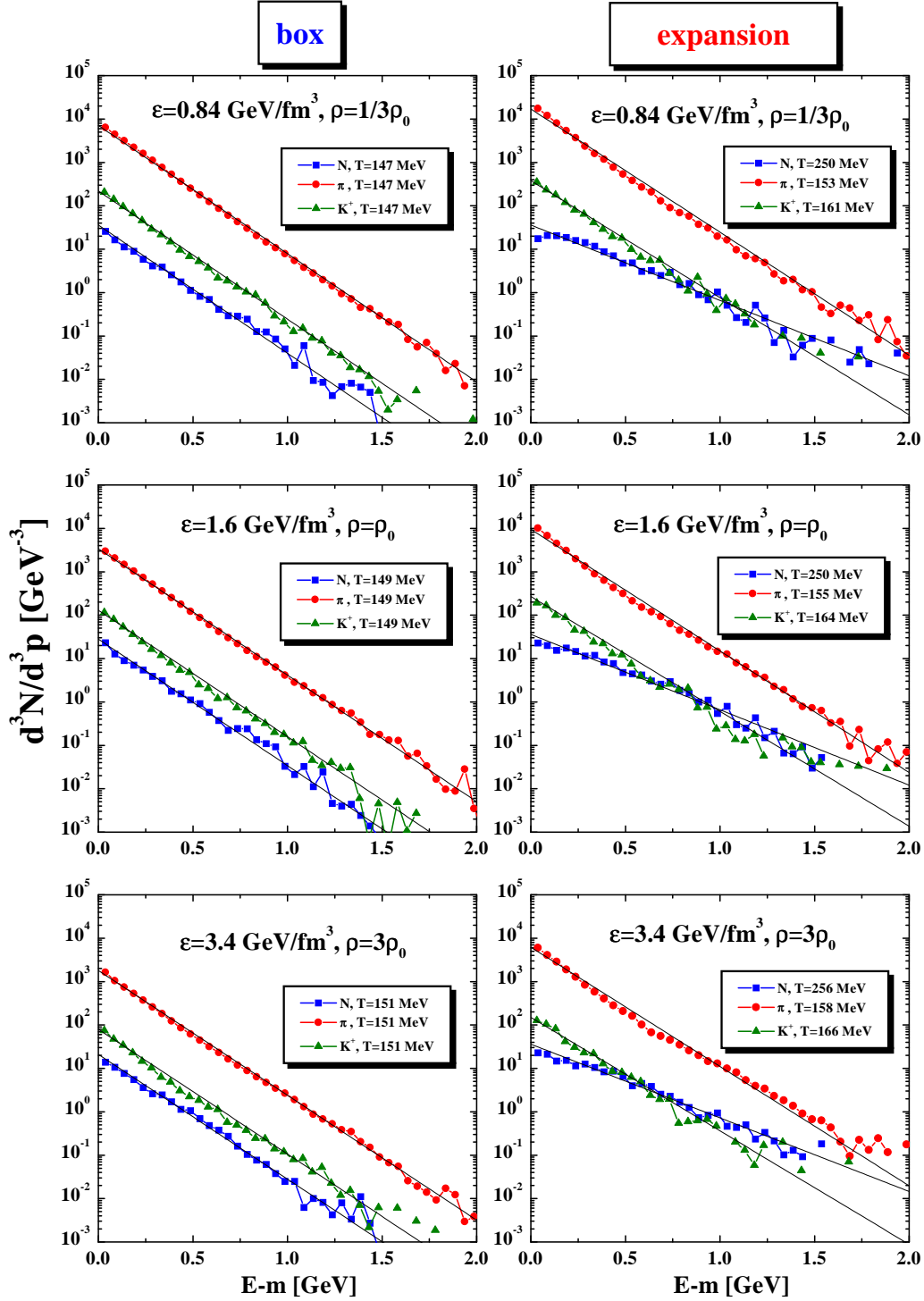
Figure 13: The spectra of nucleons (N), pions (π) and kaons (K^+) versus the kinetic energy $E - m$ before (left panel) and after (right panel) expansion for $\rho = 1/3\rho_0$ at $\varepsilon = 0.84$ GeV/fm^3 (upper part), for $\rho = \rho_0$ at $\varepsilon = 1.6$ GeV/fm^3 (middel part) and for $\rho = 3\rho_0$ at $\varepsilon = 3.4$ GeV/fm^3 (lower part).
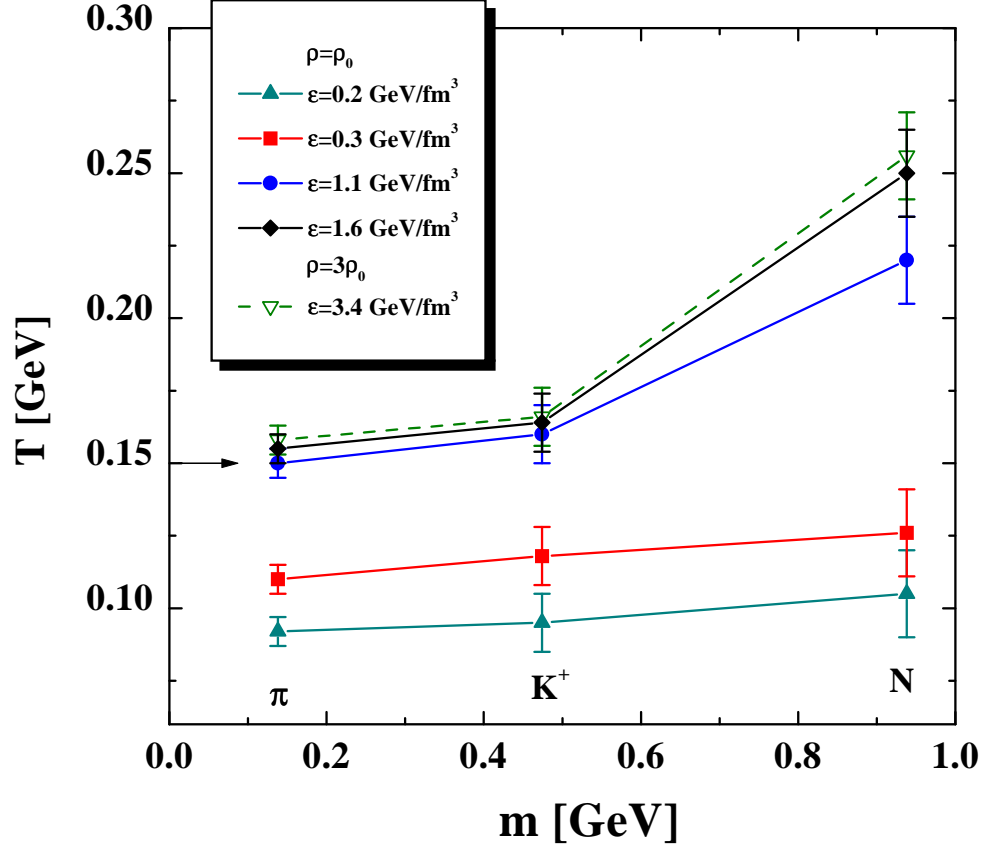
Figure 14: The spectral slope T after expansion versus the hadron mass m for π, K^+, N at $\rho = \rho_0$ and different energy densities: $\varepsilon = 0.2$ GeV/fm^3 (up full triangles), $\varepsilon = 0.3$ GeV/fm^3 (full squares), $\varepsilon = 1.1$ GeV/fm^3 (full dots), $\varepsilon = 1.6$ GeV/fm^3 (full diamonds); for $\rho = 3\rho_0$ at $\varepsilon = 3.4$ GeV/fm^3 (down open triangles). The arrow indicates the limiting temperature $T_s \simeq 150$ MeV before the expansion.
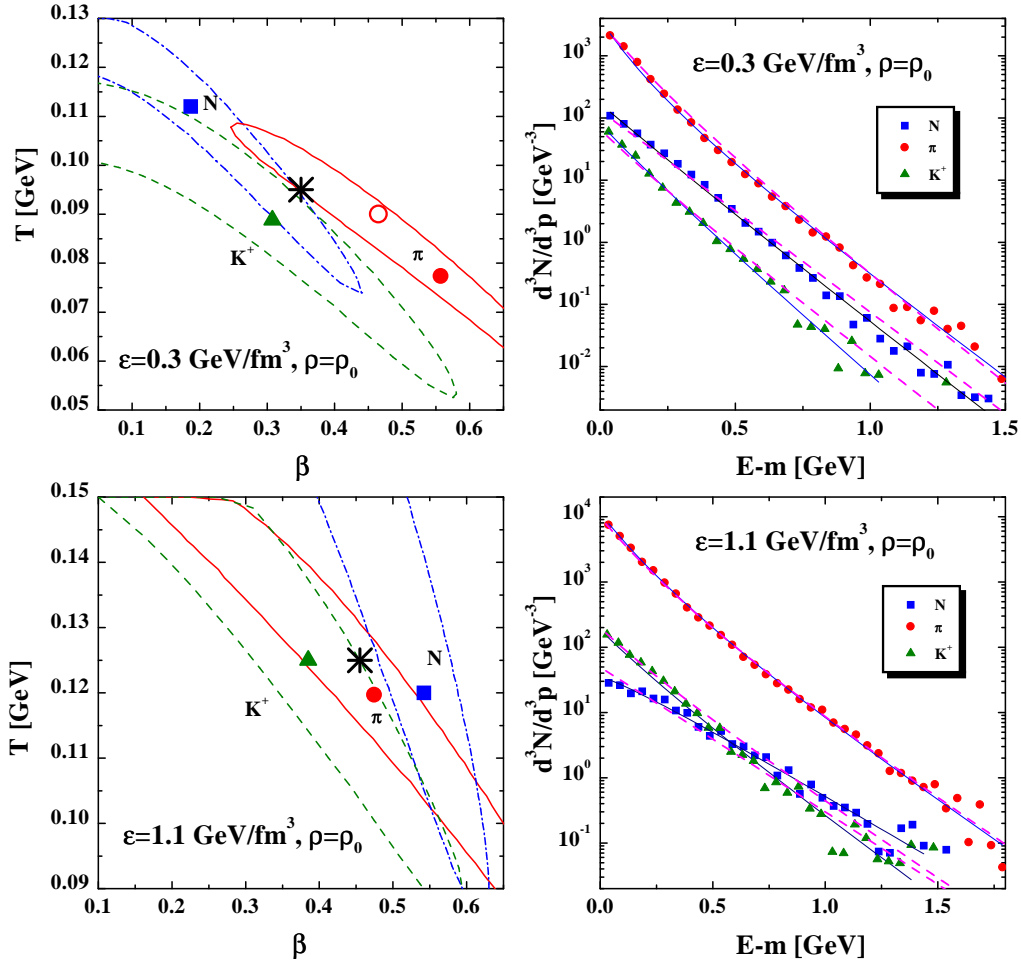
Figure 15: Left panel: the contour plots for the parameter errors in the $T - \beta$ plane; dot-dashed lines: nucleons (N), solid lines: pions (π) and dashed lines: kaons (K^+) for the energy densities $\varepsilon = 0.3$ (upper part) and 1.1 GeV/fm^3 (lower part) at $\rho = \rho_0$. The full symbols indicate the 'optimal' parameters T and β (squares for N, dots for π and triangles for K^+). The open dot (upper left plot) reflects β, T for the pion spectra including the cut-off $E - m > 0.4$ GeV. Right panel: the full symbols (squares for N, dots for π and triangles for K^+) are the box calculations (for the same ρ and ε as in the left panel). The thin solid lines show the fit of the particle spectra with the 'optimal' T and β parameters from the left panel; the dashed lines correspond to the 'eye' fit with the average β and T parameters given by the stars from the left panel.
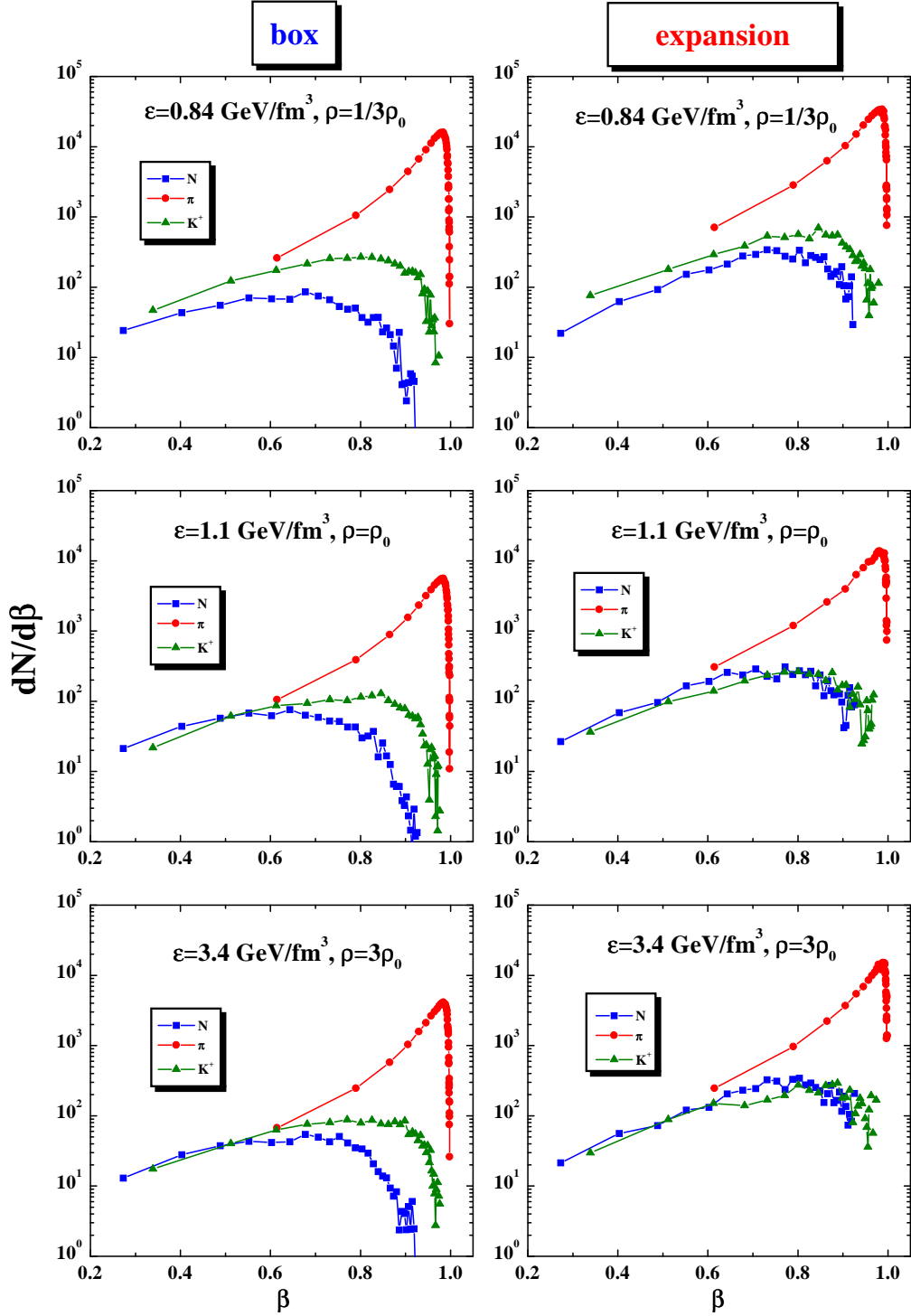
Figure 16: The velocity distributions $dN/d\beta$ for nucleons (N), pions (π) and kaons (K^+) for $\rho = 1/3\rho_0$ at $\varepsilon = 0.84$ GeV/fm^3 (upper part), for $\rho = \rho_0$ at $\varepsilon = 1.1$ GeV/fm^3 (middle part) and for $\rho = 3\rho_0$ at $\varepsilon = 3.4$ GeV/fm^3 (lower part). The left panel shows $dN/d\beta$ at equilibrium whereas the right panel corresponds to $dN/d\beta$ after the expansion phase.
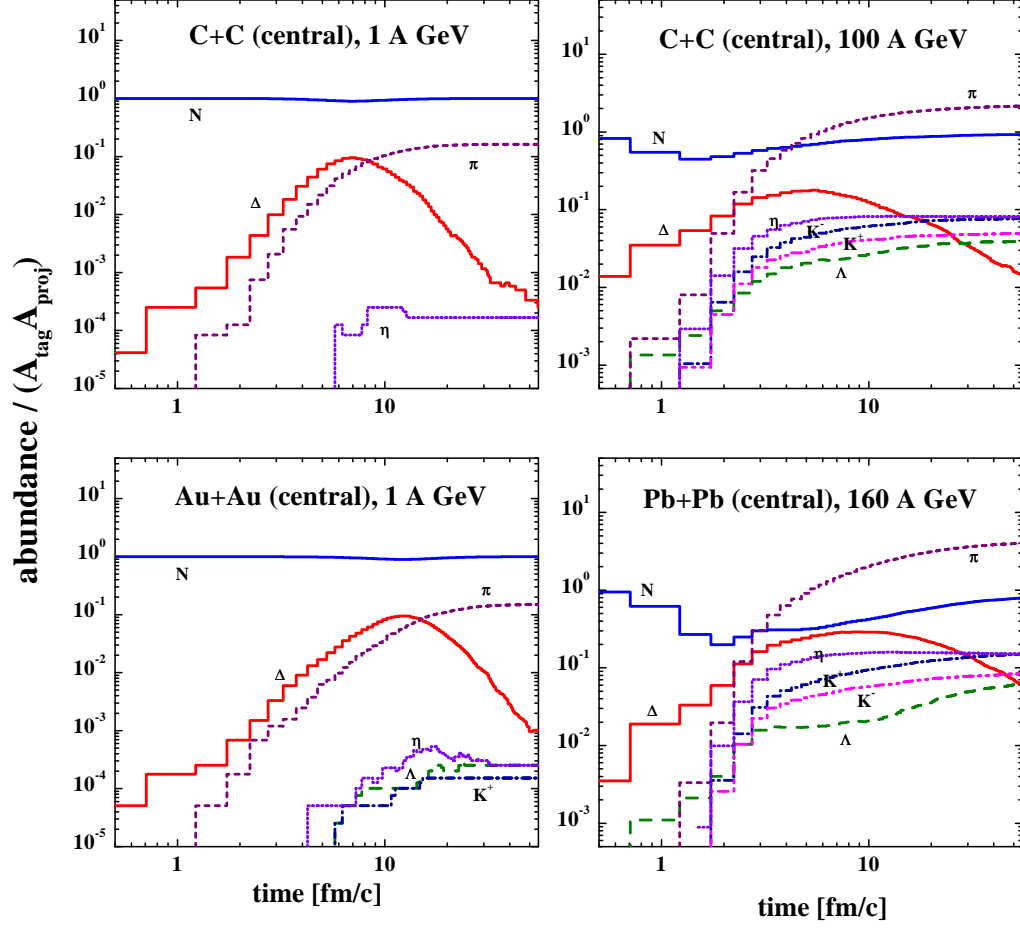
Figure 17: Time evolution of the particle abundances (nucleons N, Δ, Λ, π, η, K^+) for central C + C collisions (upper part) and Au + Au and Pb + Pb collisions (lower part) at 1 A·GeV (left panel) and 160 A·GeV (right panel).
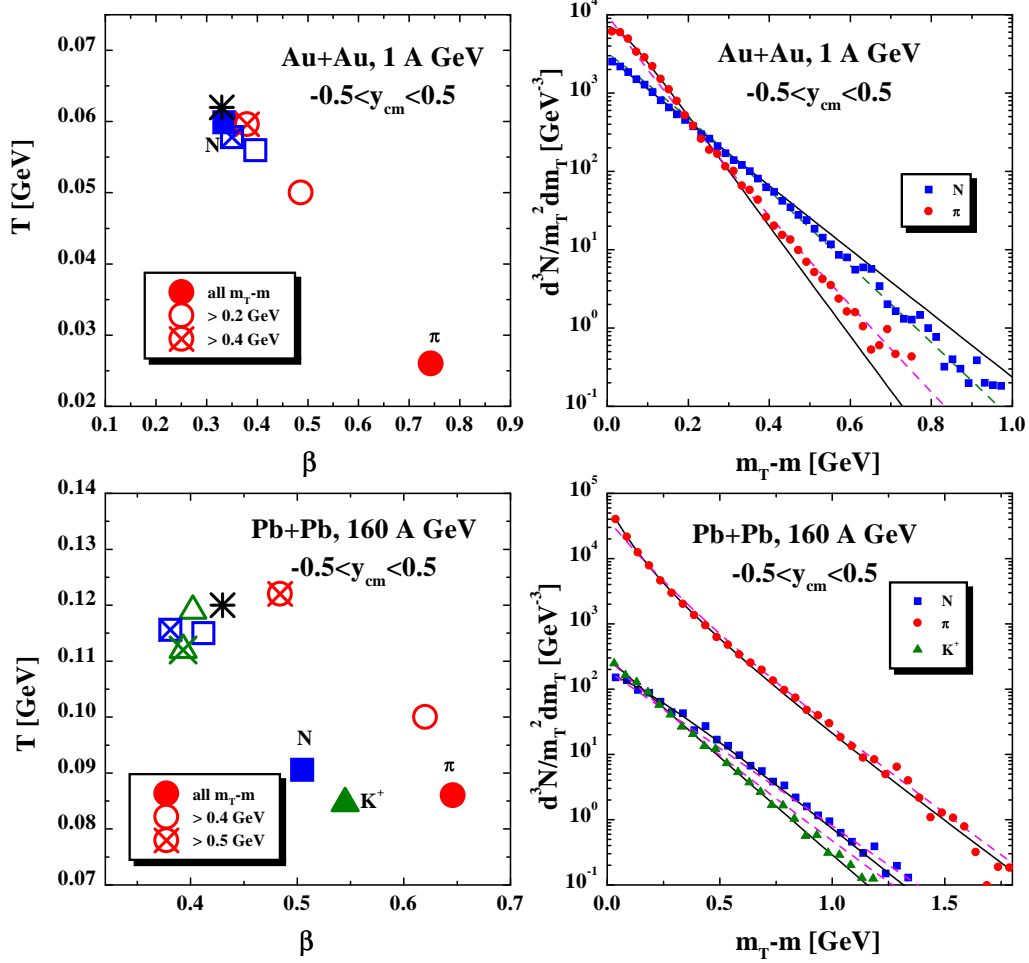
Figure 18: Left panel: the full symbols indicate the 'optimal' parameters T and β (squares for N, dots for π and triangles for K^+) obtained by exploring the full m_T spectra in the fitting procedure. The open symbols correspond to β, T for the cut-off $m_T - m > 0.2$ GeV (upper part) and 0.4 GeV (lower part); the open symbols with crosses inside indicate the β, T parameters for the cut-off $m_T - m > 0.4$ GeV (upper part) and 0.5 GeV (lower part). The stars corresponds to the β, T parameters from Ref. [41] for Au + Au at 1 A·GeV and from Ref. [42] for Pb + Pb at 160 A·GeV. Right panel: Transverse mass (m_T) spectra of nucleons (N), pions (π) and kaons (K^+) for central Au + Au collisions at 1 A·GeV (upper part) and central Pb + Pb collisions at 160 A·GeV (lower part) for $-0.5 \le y_{cm} \le 0.5$: the full symbols are the transport calculation; the thin solid lines show the m_T spectra for the 'optimal' T and β parameters from the left panel; the dashed lines show the fit with the β, T values corresponding to the 'stars' from the left panel.